Report
R-15-04
November 2018

Influence of cold work and notches on creep failure of Cu-OFP

Rui Wu
Rolf Sandström

SVENSK KÄRNBRÄNSLEHANTERING AB

SWEDISH NUCLEAR FUEL
AND WASTE MANAGEMENT CO

Box 250, SE-101 24 Stockholm
Phone +46 8 459 84 00
skb.se

SVENSK KÄRNBRÄNSLEHANTERING

ISSN 1402-3091
SKB R-15-04
ID 1468008
November 2018

Influence of cold work and notches on creep failure of Cu-OFP

Rui Wu, Rolf Sandström
Swerea KIMAB

Keywords: As-received, Cold worked, Notch, Creep crack growth, Shear, Compression, Creep damage, Interruption, Rupture.

Abstract

Four special types of creep tests have been performed for phosphorus alloyed oxygen free copper (Cu-OFP) to generate data that are needed in the stress analysis of copper canisters for spent nuclear fuel. The role of multiaxial stress states are covered in three of the tests. Notched round bar specimens, compact tension (CT) specimens, and shear specimens were used. The fourth type was uniaxial compression tests. For all types of specimens as received material was used except for the notched round bars, where a 24% cold worked condition was studied. Two compression tests were also carried out for this condition.

All the test of the notched round bar specimens were interrupted before rupture. The test results demonstrate that the increase in creep strength is as least 30%, i.e. the same amount as for uniaxial specimens when 24% cold worked Cu-OFP is compared with as received material. This means that there is no notch weakening and that the reference stress method does not overestimate the creep strength of the notched specimens.

Tests of CT specimens were performed at 75, 100, 125 and 175°C. Four specimens were tested without side grooves, one at each temperature. For comparison one specimen at 125°C did have side grooves. All tests were interrupted before rupture. Only the specimen with side grooves showed crack propagation. A previously published model (Wu et al. 2013) could fully describe the difference between specimens with and without side grooves. The presence of side grooves increases the constraint around the notch and thereby the presence of multiaxial stresses. The results show that the risk for crack initiation and propagation increases dramatically when notches are highly constrained.

Flat specimens with notches oriented in such way that the ligament between them was exposed to a large shear stress were creep tested. The stress and strain distributions in these specimens were analysed with FEM software. The specimens could be exposed to high local stresses and strains before rupture. This shows that Cu-OFP is not notch sensitive under shear load.

Four cylindrical specimens were creep tested in compression at 75°C, two for as-received Cu-OFP and two for bar material that had been strained in tension at room temperature to 24%. The four specimens showed about the same creep strain versus time behaviour. The absence of the influence of the cold work is consistent with the corresponding results in uniaxial tension when the deformation and testing directions are opposite. The observed creep strain in compression is much lower than the corresponding strain in tension at the same stress level. This difference could be explained with a model for primary creep when taking the difference in stress state into account.

Contents

1 Introduction

Phosphorus alloyed oxygen free copper (Cu-OFP) canisters have been selected for spent nuclear fuel disposal in the Swedish nuclear waste programme (Rosborg and Werme 2008). In the repository the copper canisters will be exposed to external hydrostatic pressure and swelling from the surrounding bentonite at temperatures estimated to be up to about 100°C. The copper canister will be deformed by creep under multiaxial stress states (Sandström and Andersson 2008, Sandström 2012). To ensure the integrity of the copper canister, sufficient creep ductility must be maintained, especially for critical positions subjected to cold work such as where indentation appears.

Failure mechanisms, modes and strain (ductility) are found to be affected by the stress state (Dyson and Loveday 1981, Hayhurst and Webster 1986, Hayhurst and Henderson 1973). Under high degrees of tensile multiaxility premature failure can occur due to the inhibition of deformation and enhancement in the fracture processes (Dyson and Loveday 1981). Ductility can decrease significantly for notch sensitive materials. High degrees of multiaxility can be found at notch roots.

One established method of introducing a state of multiaxial stress into laboratory specimens is to subject circumferentially round notched bars to an axial tensile stress (Webster et al. 1992). Using notched bar specimens, creep tests have been conducted for Cu-OFP (Wu et al. 2009a, b). It has been shown that the Cu-OFP is insensitive to notches at 75°C. Actually, the creep lifetime under multiaxial stress state is longer than that under uniaxial stress state at a given net section stress. This indicates notch strengthening at the given net section stress. The sharper the notch, the longer the creep lifetime at a given net section stress. The rupture life of notched and unnotched specimens was the same for the same reference stress (Wu et al. 2009a, b). Using a fundamental creep model without fitting parameters, it was possible to represent the creep strain curves for the notched specimens quite well (Wu et al. 2009a, b).

Few studies of creep crack growth (CCG) are available for Cu-OFP (Seitisleam and Henderson 1997, Andersson 2005, Wu and Seitisleam 2010, Wu et al. 2013). Seitisleam and Henderson (1997) showed that some local crack growth had taken place near the notched region. Other studies (Wu and Seitisleam 2010, Wu et al. 2013) exhibited that crack did grow by creep about 10 mm before final instantaneous failure at 175 and 215°C, leading to premature failure in comparison to that of uniaxial creep tests at the same reference stress. At 75°C and lower, there was hardly any visible crack growth. Modelling of CCG using CT specimens has also shown that, due to creep, the high stresses are rapidly relaxed and a homogeneous stress across a band of the specimen is formed.

On cold worked copper with high oxygen content, Auerkari et al. (2005) carried out multi-axial interrupted creep test using sharp notches in compact tension (CT) specimens. They did find separate intergranular creep cavities near the notch tip, in addition to a distinct grain boundary zone with elevated P content, also near the notch tip. Auerkari and co-workers reported also CCG testing results on a Cu-OFP friction stir weld at 175°C (Auerkari et al. 2009). After 15,000 h, the main crack started to initiate and showed intergranular branching perpendicular to the nominal tensile principal stress. They thought that the crack initiation and branching were associated with metallurgical and defect-specific features as well as the impact of multi-axial stress state.

The slit between the welded tube and lid in copper canisters represents a stress concentration. It has been demonstrated that the most severely deformed sections in the copper shell lie in the slit roots, particularly in unevenly loaded copper shells (Jin and Sandström 2013). In the slit roots von Mises stresses up to 238 MPa emerge. However, the stresses in the slit roots are compressive. Generally, there is experience that creep tests of ductile metallic materials do not fail in compression.

Using round notched bars, the magnitude of both strains in compression and tension in the slits can be simulated. However, strain distributions around sharp notches are not quite the same as those in the canister slits. For this reason another type of test, shear test using shear specimens, has been carried out. In the shear specimen the notches are placed at 45° angle to the loading direction. Simulation of transverse and the axial plastic strains are illustrated in Figure 1-1. They show the largest strain on the side of the notches.

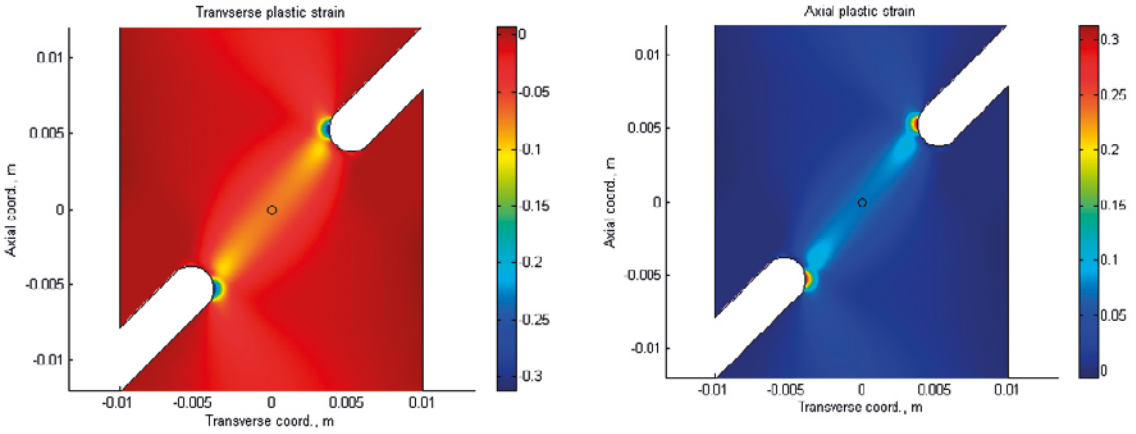

Figure 1-1. *Shear specimen. Axial tensile load corresponding to an average stress at the specimen ends of 95 MPa. a) Transverse plastic strain. b) Axial plastic strain.*

2 Purpose of the project

The purposes of the present work are to

1) conduct different creep tests on Cu-OFP under multiaxial conditions,
2) conduct different creep tests on cold-worked Cu-OFP,
3) provide creep data for verification of constitutive equations, and
4) simulate the behaviour of slits in copper canister.

3 Materials and experiments

3.1 Material

The Swedish Nuclear Fuel and Waste Management Co (SKB) supplied test material with SKB internal identity T48-R2, which was taken from an extruded tube made of phosphorus alloyed oxygen-free copper (Cu-OFP). This material is considered as as-received material. The chemical composition is given in Table 3-1 (SKB 2010). The mean grain size (three measurements) of top and bottom of the extruded tube was approximately 240 and 60 µm, respectively (SKB 2010). Elongation at room temperature was greater than 40% (SKB 2010).

Table 3-1. Chemical composition of the investigated extruded tube made of Cu-OFP. All are mean values and given in wtppm, except for Cu (in wt%).

Cu	P	Ag	As	Bi	Cd	Fe	H	Mn	Ni	O
99.99	69	13.4	0.82	0.12	< 0.003	1.4	0.4	< 0.1	0.85	1.1
Pb	**S**	**Sb**	**Se**	**Sn**	**Te**	**Zn**				
0.27	4.4	0.06	< 0.09	0.06	0.05	< 0.1				

Both as-received and 24% cold worked materials were tested in the present study. Material cold worked to 24% was obtained by first extracting cylindrical bar specimens with threaded ends from the as-received tube material. Second, the cylindrical bar specimens were subjected to 24% deformation in tension. This action represents 24% cold working. Figure 3-1 shows the 24% cold worked specimen that was used for manufacturing of cylindrical, double notched creep specimens as well as columnar compression specimens. Mean hardness values of the as-received and the 24% cold worked materials were HV76 and HV105, respectively (average of six measurements).

3.2 Design and dimension of various specimens for creep tests

3.2.1 Cold worked (24%) cylindrical, double notched creep specimen

Two notches were introduced on the 24% cold worked cylindrical specimen with threaded ends, see Figure 3-2. The introduction of the notches will create a multiaxial stress state at the notches when subjected to tensile load. The notch acuity, a/R, was chosen to 5. The parameter a is the radius of the specimen at the base of the notch position in mm, and R the notch root radius in mm. In the present case, a/R = 2.82/0.564 = 5. The ratio of b/a was set to $\sqrt{2}$. The parameter b is the gross radius of the specimen. Its value was 3.988 mm, see also Figure 3-2. The dimensions of the specimen correspond to those recommended in the code of practice for notched bar testing (Webster et al. 1992).

Only the 24% cold worked material was used for the notched bar creep tests.

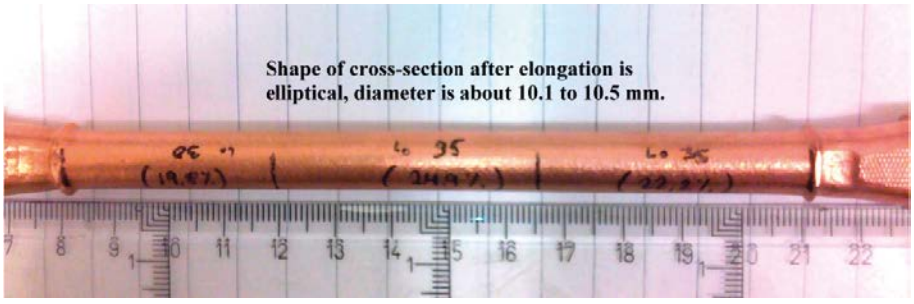

Figure 3-1. *Cylindrical bar specimens after 24% cold work to be used for manufacturing of cylindrical, double notched creep specimens.*

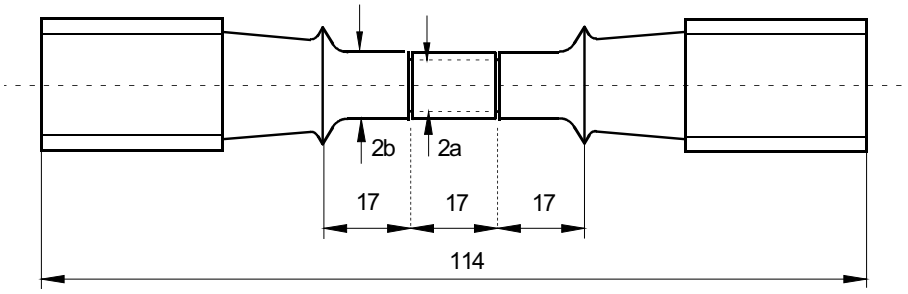

Figure 3-2*. 24% cold worked cylindrical, double notched creep specimen. The notch acuity, a/R, was 5. a is the radius of the specimen at the base of the notch position, and R the notch root radius.*

3.2.2 Compact tension (CT) specimen

Standard compact tension (CT) specimens with and without side grooves were used for the creep crack growth (CCG) tests. Figure 3-3 shows a CT specimen with side grooves. For the CT specimen without side grooves both sides were flat. The geometry of the CT specimen having a width W of 50 mm and a full thickness B of 25 mm is given in Figure 3-4. The spark machined notch has a root radius of 0.15 mm.

The applied load was calculated using the reference stress concept. A common way of defining the reference stress in MPa (σ_{ref}) for a CT specimen is given below (Miller 1988; Chorlton M 1999, personal communication). The choice of reference stress also refers to previous results (Wu et al. 2013).

$$\sigma_{ref} = \frac{P}{m \cdot B_{eq} \cdot W} \qquad \text{(Equation 3-1)}$$

where

$$m = -(1 + \gamma(\frac{a}{W})) + \sqrt{(1+\gamma)(\gamma(\frac{a}{W})^2 + 1)} \qquad \text{(Equation 3-1a)}$$

and

$$B_{eq} = B - \frac{(B - B_n)^2}{B} \qquad \text{(Equation 3-1b)}$$

and

$$\gamma = \frac{2}{\sqrt{3}} \qquad \text{(Equation 3-1c)}$$

where P is the load in N, a the crack length in mm, W the length from the centre of the load-pin hole to the back of the specimen in mm, B the width of the specimen in mm, and B_n the net thickness between the side grooves in mm. Note that σ_{ref} changes (increases) as the crack extends (a increases). The exact dimensions of each CT specimen were measured prior to test and are given in Table 3-2, together with the initial reference stress σ_{ref} and initial applied load.

Only the as-received material was used for CCG test.

(a) (b)

Figure 3-3. *Standard compact tension (W = 50 mm) specimen with side grooves for CCG testing. (a) Side-view and (b) back-view.*

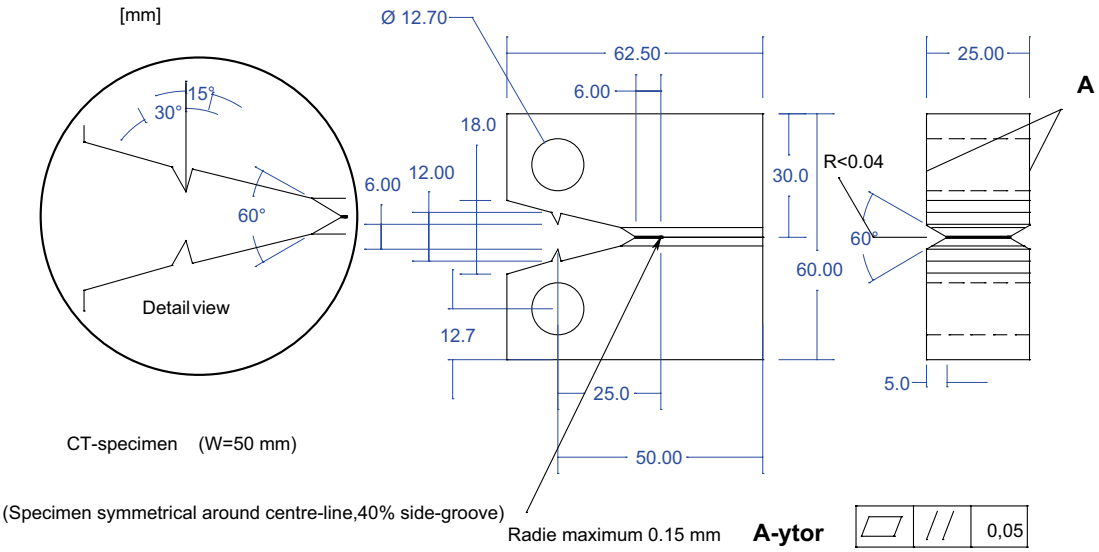

Figure 3-4. *Geometry of compact tension (CT) specimen having W = 50 mm and side grooves.*

Table 3-2. CT specimen geometry, initial reference stress σ_{ref} and initial applied load.

Specimen#	W* (mm)	B_n* (mm)	B_{eq}** (mm)	a* (mm)	W-a* (mm)	Initial σ_{ref} (MPa)	Initial load (N)
CCG175	50.095	25.112	25.112	22.712	27.383	115	15,813.3
CCG125-1	50.075	25.055	25.055	22.528	27.547	165	22,965.6
CCG125-2	49.663	14.913	20.973	21.709	27.954	170	20,719.1
CCG100	49.978	25.037	25.037	22.537	27.441	185	25,567.0
CCG75	50.053	25.048	25.048	22.681	27.372	195	26,750.7

All the CT specimens were without side grooves, except for the specimen CCG125-2.

* Measured value.

** Calculated value according to Equation 3-1b.

3.2.3 Flat shear specimen

The flat shear specimen was designed to represent the slits in the copper canister. Although the notched bar specimens can simulate the magnitude of both the strains in compression and tension in the slits, the strain distributions around the sharp notches are not the same as in the canister slits. In the shear specimens, the strain distributions are somewhat closer. In the flat shear specimen the notches were placed at 45° angle to the loading direction, see Figure 3-5. The centre of the flat shear specimen is exposed to shear stresses under tension. The specimens had a width of 20 mm and a thickness of 5 mm. The specimens were machined from round bars.

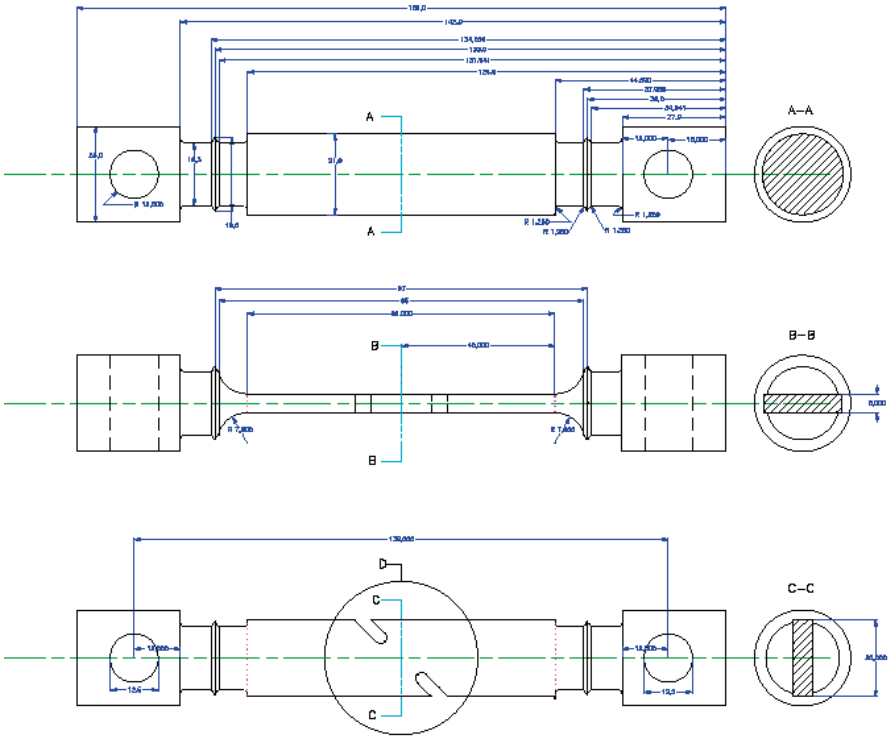

(a) Geometry

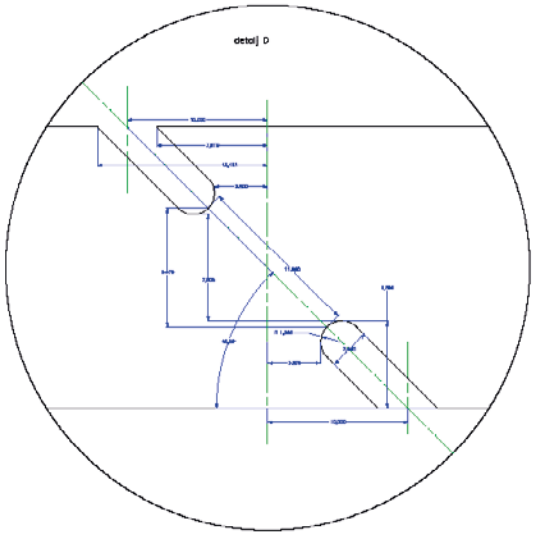

(b) Detail of 45° notch

Figure 3-5. *Flat shear specimen for shear test.*

Figure 3-6(a) shows examples of the flat shear specimens. The 45° notches were white painted with a net in order to observe the deformation around the notch, see Figure 3-6(b). The overall strain was measured between two edges, see Figure 3-6(a).

Only the as-received material was used for the shear tests. The nominal stress for the specimens was obtained as the load divided by the cross section away from the notches.

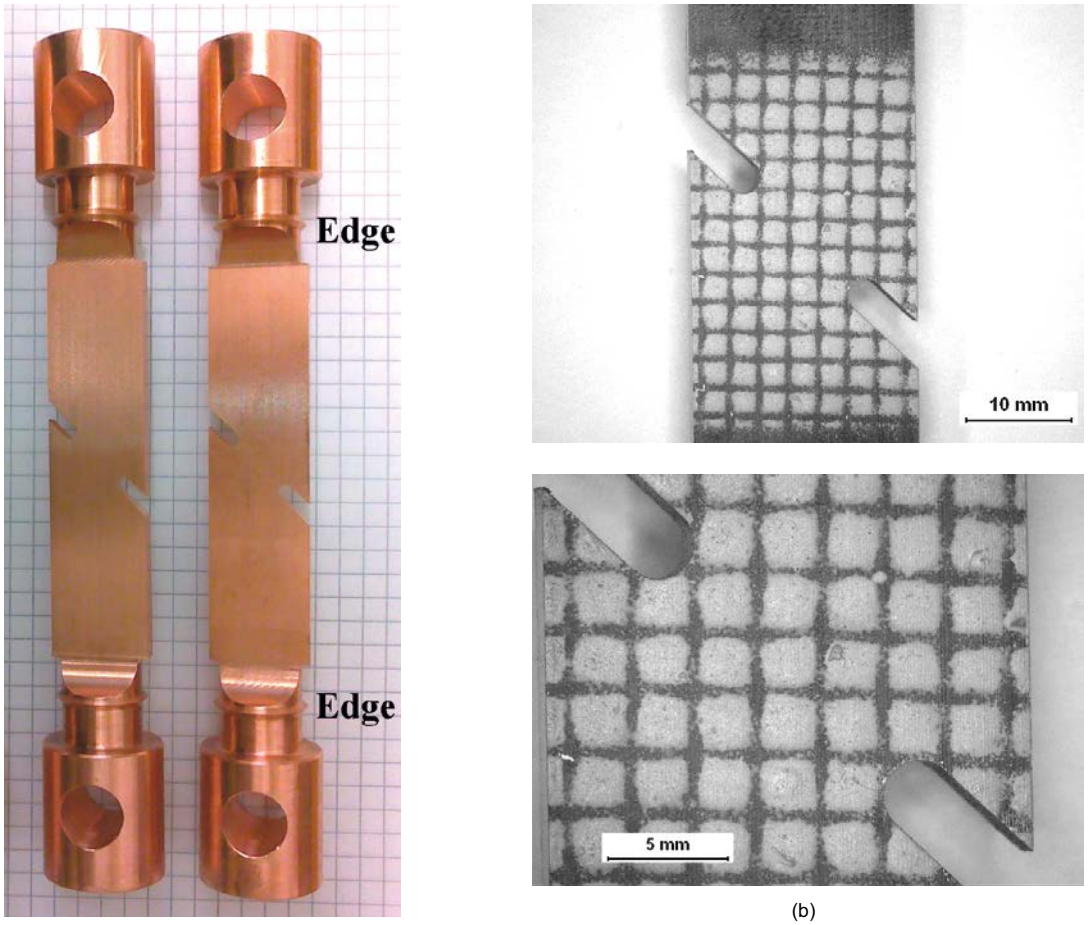

Figure 3-6. *Prior to test. (a) Flat shear specimens and (b) White painted measuring net around the notch.*

3.2.4 Columnar specimen

Columnar specimen with 10 mm in diameter and 10 mm in height were used for compression tests, see Figure 3-7.

Both the as-received and the 24% cold worked materials were used for the compression tests.

3.3 Creep testing

Generally, creep strain, time and temperature were periodically recorded by a logger. For the CT specimens, potential drop (PD) and load line displacement (LLD) were also recorded. The maximum temperature variations with time were controlled within ± 2°C of target temperatures. The applied load and load variation obeyed the requirements in the standard (ISO EN 204 2005).

3.3.1 Creep testing using notched creep specimen

Single specimen, constant dead load creep testing machines were used for the 24% cold worked cylindrical, double notched creep specimen shown in Figure 3-2. Four tests were isothermally conducted at a constant temperature of 75°C at different initial net section stresses. The net section stress is the applied axial load divided by the minimum cross section at the notch. Uniaxial load was axially applied on the specimens with measurement of the displacement over the whole gauge length of 51 mm, see Figure 3-2. All tests were interrupted before rupture due to unexpectedly long test duration.

3.3.2 Creep crack growth (CCG) testing using CT specimen

Five CCG tests have been conducted at 75, 100, 125 and 175°C in air at different initial reference stresses. The CT specimens did not have side grooves, except for one test at 125°C, see Figure 3-3. The CCG tests followed a draft of the standard ASTM E-1457-98. This draft has been standardised since 2007. The tests were conducted in a dead load creep test rig modified for CCG tests. The CCG test assembly is given in Figure 3-8. The direct current potential drop (PD) method monitored the crack progress and a purpose-built extensometer was used to measure the load line displacement (LLD) and notch tip opening.

Potential drop measurements work in such a way that a constant direct current is led through the specimen across the crack propagation plane. The potential differences across the same propagation plane are then measured and recorded. As soon as the crack grows, the cross section area is reduced. Under the constant current condition, the potential will increase accordingly. There is an equation to calculate the crack length advance using PD recordings (ASTM E-1457-98).

Because of the good electrical conductivity of copper, there are difficulties in PD measurements, especially if the changes in PD are small. To minimise these difficulties, some considerations such as full size CT specimen, white painted measuring net and protection of electrical contacts were taken (Wu et al. 2013).

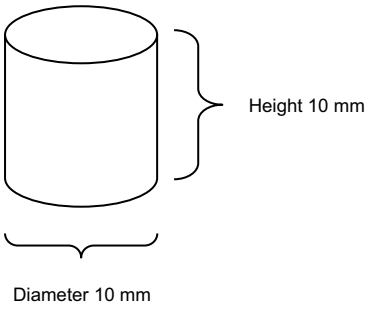

Figure 3-7. *Columnar specimen for compression test.*

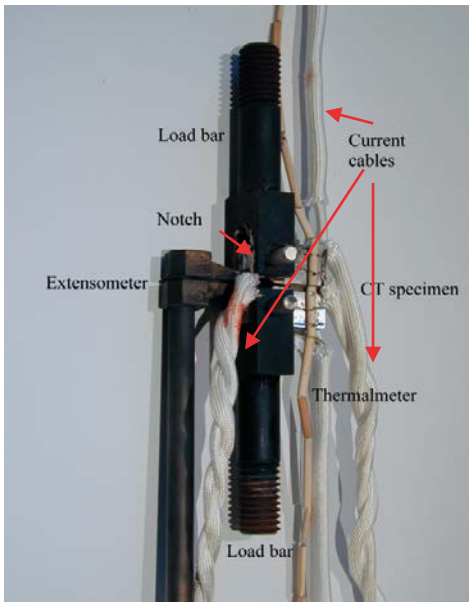

(a)

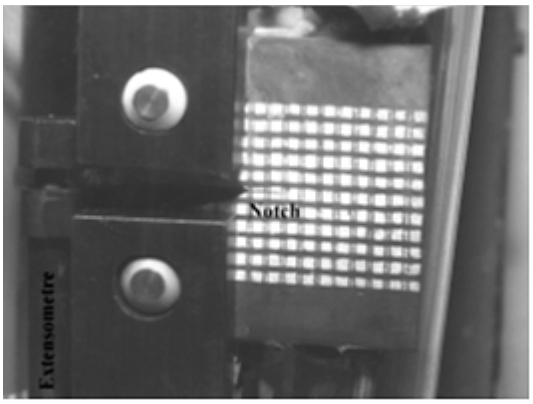

(b)

Figure 3-8. *(a) Assembly of CT specimen. (b) White painted CT specimen with measuring net.*

The reference stress was gradually increased in order to initiate crack propagation in some tests. Images of notch tip opening and crack tip appearance were regularly taken before, during and after CCG tests.

For the test with side grooves at 125°C, a damper was installed with the load bar on the test rig to minimise vibrations, see Figure 3-9.

3.3.3 Shear testing using flat shear specimens

Two shear tests using the flat shear specimen shown in Figure 3-6 were performed at 75°C using single specimen, constant dead load creep testing machine. The stress was determined using the minimum area across the notches. Before the testing a net of lines was placed on the specimens. Images of notch tip opening and notch tip appearance were regularly taken during the tests. In this way the deformation around the notches could be followed. One test failed and one was interrupted.

3.3.4 Compression testing using columnar specimen

Four compression tests, two for as-received and two for 24% cold worked material, were carried out at 75°C, 180 MPa using single specimen, constant dead load creep testing machines. A set of specimen holder with two parallel plates was developed and used to keep the columnar specimen at the centre of the plate. When a tensile load is applied, the upper and the lower plate will move downwards and upwards, exerting a compression on the columnar specimen, see Figure 3-10.

3.4 Post test metallographic examination

After creep testing, interesting parts were cut from selected specimens, mounted, ground and polished to 0.25 µm, and finally etched in a solution containing 40 g CrO_3, 7.5 g HN_4Cl, 50 ml H_2SO_4, 50 ml HNO_3 and 1,900 ml H_2O. Creep damage examinations on the etched metallographic samples were performed using the Leica light optical microscope (LOM).

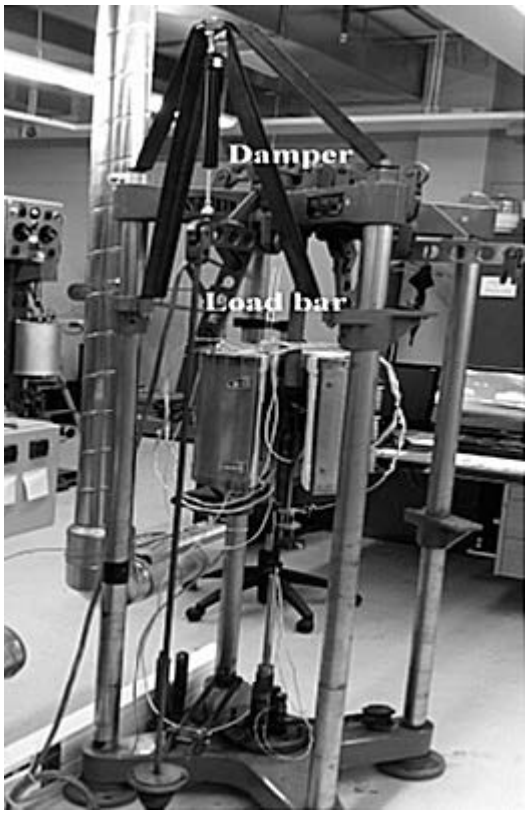

Figure 3-9. *Creep test rig equipped with damper for the CCG test using CT specimen with side grooves at 125°C.*

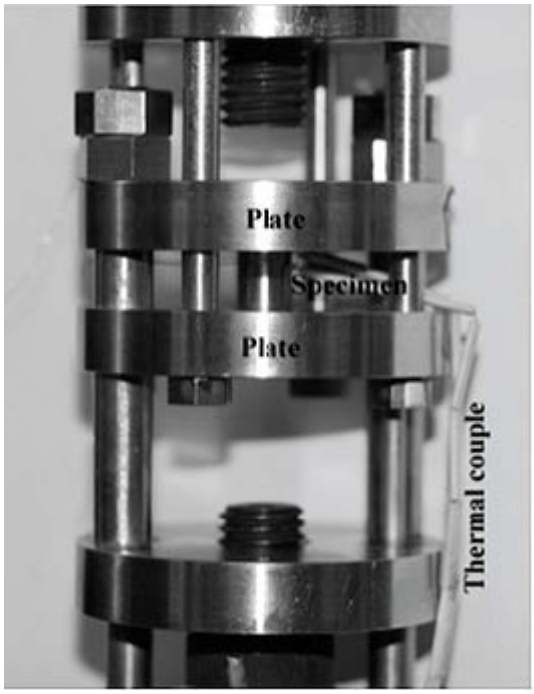

Figure 3-10. *A set of holder with two parallel plates for compression test.*

4 Creep test results

The creep test matrix is exhibited in Table 4-1. Four different types of tests were conducted, 1) four creep tests using notched specimen with 24% cold worked material at 75°C, 2) five CCG tests using CT specimens with or without side grooves for the as-received material at 75, 100, 125, and 175°C, 3) two shear tests using the flat shear specimen for the as-received material at 75°C, and 4) four compression tests at 75°C, 180 MPa using columnar specimens for as-received and 24% cold worked material. All the CT specimens were without side grooves, except for the specimen CCG125-2. All the tests were interrupted, either due to unpredictable long testing time, or due to the move of the creep laboratory. Only one shear test at 80 MPa ruptured.

Table 4-1. Creep test matrix.

Type of test	Specimen designation	Stress (MPa)	Temp (°C)	Time at interruption, t_{IR} (h)	Strain at interruption, ε_{IR} (%)	Load line displ. LLD (mm)	Uploading strain (%)	LLD under uploading, (mm)
Notched, 24% cold worked	Cu24-5-1	245	75	7,246	0.040		0.076	
	Cu24-5-4	285		8,327	0.070		0.129	
	Cu24-5-5	295		6,743	0.131		0.178	
	Cu24-5-3	305		3,429	0.095		0.161	
CCG, as-received	CCG175	115**	175	12,286		3.21		6.31
	CCG125-1	165**	125	2,256		2.36		12.73
	CCG125-2^	170**	125	1,577		5.29^^		11.07
	CCG100	185**	100	2,925		2.72		13.71
	CCG75	195**	75	7,918		3.49		12.93
Shear, as-received	Shear80	80	75	4,814*	11.3		6.69	
	Shear75	75		7,798	4.978		4.62	
Compression, as-received	CP-AR-01	180	75	4,771	1.21		13.36	
	CP-AR-04	180		3,381	1.52		13.23	
Compression, 24% cold worked	CP-24-02	180	75	2,253	2.19		10.04	
	CP-24-03	180		3,428	0.944		11.23	

* Specimen ruptured.

** Reference stress in MPa calculated according to Equation 3-1.

^ With side grooves.

^^ Inaccurate LLD value due to detachment of extensometer.

4.1 Notch creep tests for 24% cold worked material

Notched creep test results for 24% cold worked material are given in Table 4-1. All four tests were interrupted since they could have taken very long time to rupture. Creep strain as a function of time is shown in Figure 4-1, including a notched test having the same notch acuity for the as-received material at 245 MPa (Wu et al. 2009a, b) for comparison. It is seen that creep strain increases slowly with time. The higher the net section stress, the higher the creep strain at a given time. Compared with the as-received notched material, the notched 24% cold worked material shows much longer creep lifetime, lower creep strain and strain rate. For instance, at 245 MPa, the as-received notched specimen failed after 20 hours, while the 24% cold worked notched specimen lasted more than 7,000 hours without any indication of failure. Since creep lifetime for as-received notched material is longer than that for the plain as-received one at a given net section stress, meaning notch insensitiveness (Wu et al. 2009a, b), the 24% cold worked material is not notch sensitive either. It is not clear why the creep strain increases suddenly at approximately 500 hours for the test at 295 MPa, see Figure 4-1. It seems, however, that creep strain rate falls back.

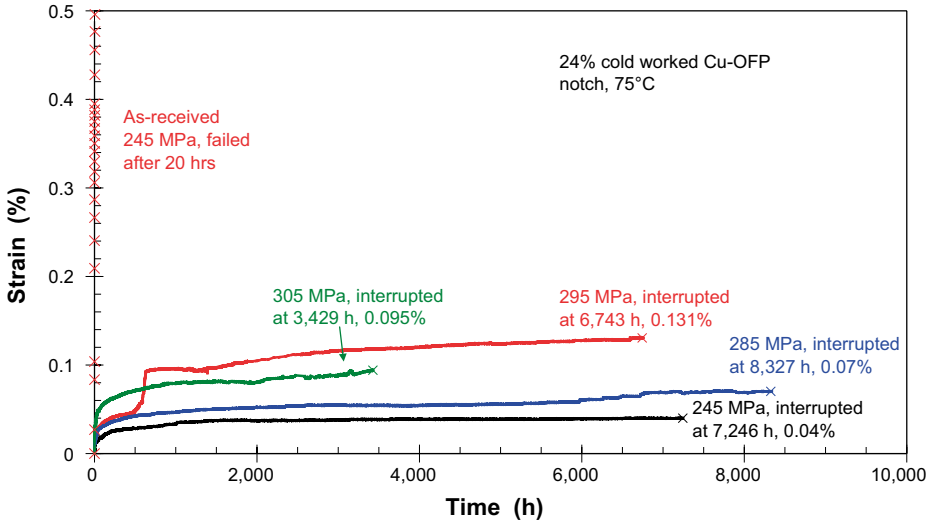

Figure 4-1. *Creep strain as a function of time for notched and 24% cold worked material at 75°C. A notched test having the same notch acuity for the as-received material at 245 MPa (Wu et al. 2009b) is included for comparison.*

4.2 CCG tests for the as-received material

For all the CCG tests it can be seen from Table 4-1 that notch tip opening (pre-LLD) occurs, from about 6.3 mm for the specimen CCG175 to over 12 mm for other specimens at full loading. The significant notch tip opening causes *i)* change of root radius of the notch, i.e. makes it greater than 0.15 mm, and *ii)* large plastic deformation and work hardening around the crack tip.

4.2.1 CCG test using CT specimen without side grooves at 175°C/115 MPa

LLD and normalised potential drop (V/V_0) as a function of time are shown in Figure 4-2. V_0 is the initial voltage at time t = 0 and V the output voltage at time t. LLD increases rapidly immediately after full loading. Increment of LLD slows down gradually so that a constant LLD rate of approximately 0.072 µm/h is obtained. The test was interrupted at 12,268 hours when LLD = 3.21 mm. Figure 4-3 shows the images of crack (notch) tip opening during the test. No crack growth could be observed. This indicates that there is a long incubation period for crack initiation at the given test condition.

4.2.2 CCG test using CT specimen with and without side grooves at 125°C

LLD and V/V_0 as a function of time are displayed in Figure 4-4 for CCG tests using CT specimens with and without side grooves. Both tests were interrupted, see Table 4-1. For the test at 170 MPa with side grooves, the load bar level have been readjusted twice because of fastened damper and inclined load bar level, which reduced the applied load. After readjustment of load bar level, the test was restarted and LLD increased rapidly immediately after full loading. Fortunately, the LLD decelerated and the LLD rate fell down to the previous level. At interruption, the LLD rates for the test with and without side grooves were 0.401 µm/h and 0.004 µm/h.

The V/V_0 recordings for the test with side grooves were to a large extent unchanged, although they fluctuated. Disturbances from the electrical supply system caused abrupt drops and jumps, see the blue line in Figure 4-4.

Figure 4-5 shows the side view of crack tip for the test with side grooves. At the full load, the notch root radius has been changed and a wedge crack has formed, see Figure 4-5(b). This wedge crack continues to develop during the testing. At interruption, the wedge crack had widened and advanced further, see Figure 4-5(f). However, this test was interrupted because unexpected reduced LLD and forced unloading and restarting of test, see Figure 4-4.

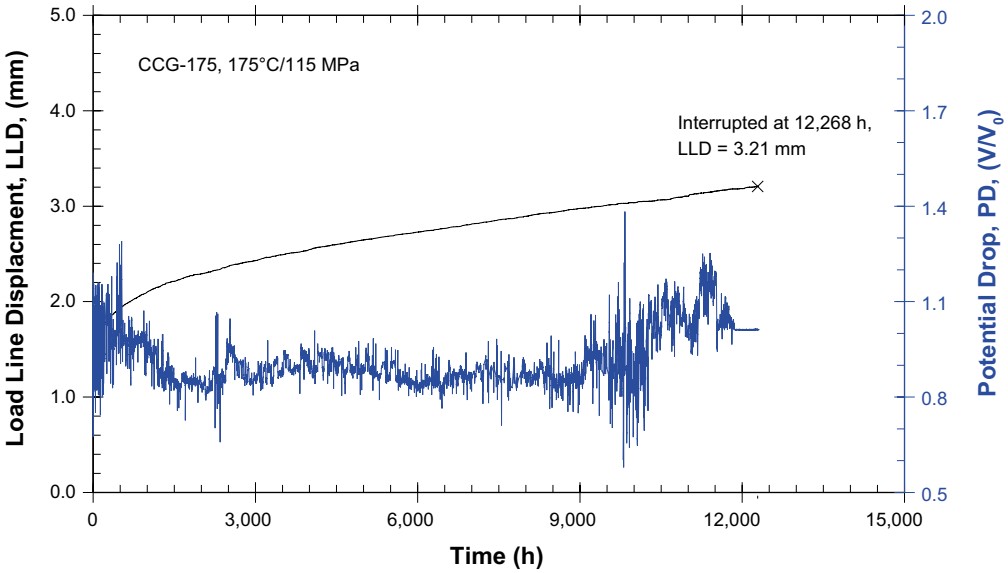

Figure 4-2. *Load line displacement (black line) and normalised potential drop (blue line) as a function of time for CCG test at 175°C/115 MPa. The test is interrupted at 12,268 h and LLD is 3.21 mm.*

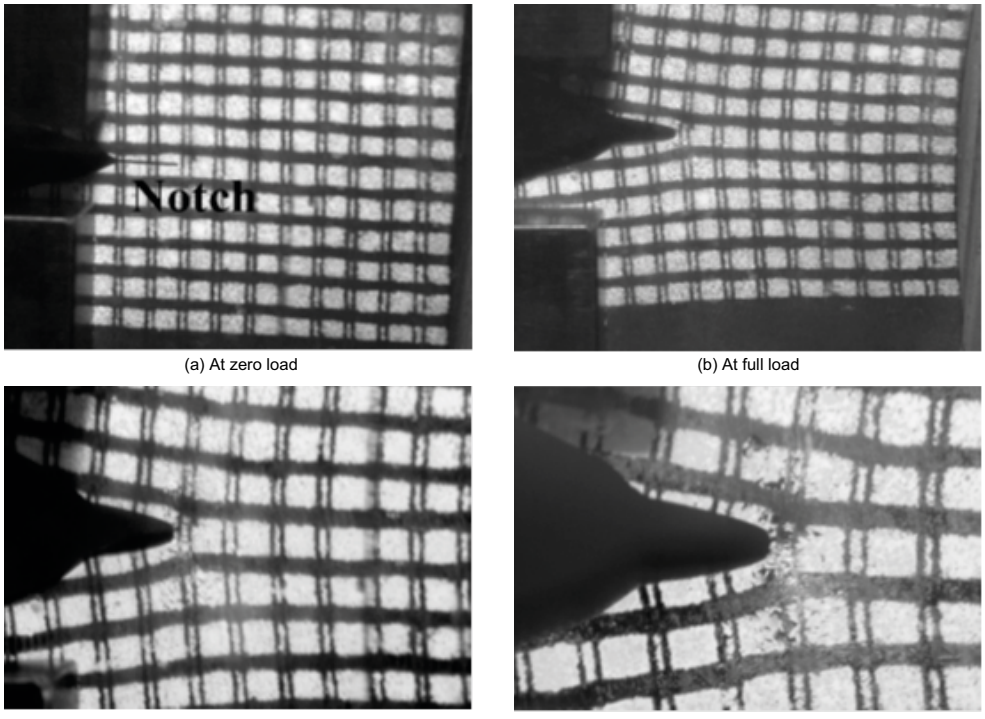

Figure 4-3. *Side view of notch tip opening at given time and corresponding LLD. CCG test at 175°C/115 MPa. The distance between the lines in the net is 2.5 mm before deformation.*

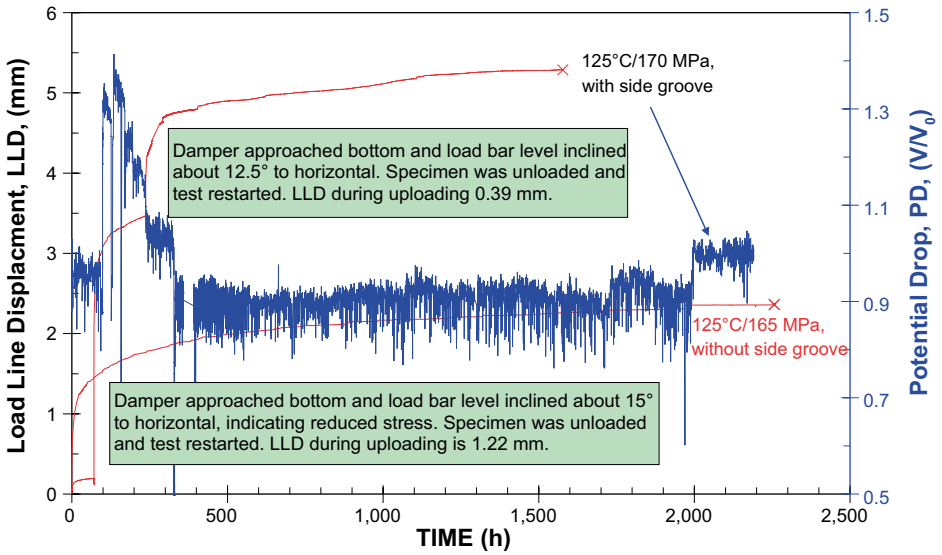

Figure 4-4. *Load line displacement (red lines) and normalised potential drop (blue line, with side grooves) as a function of time for CCG tests at 125°C. Both tests were interrupted.*

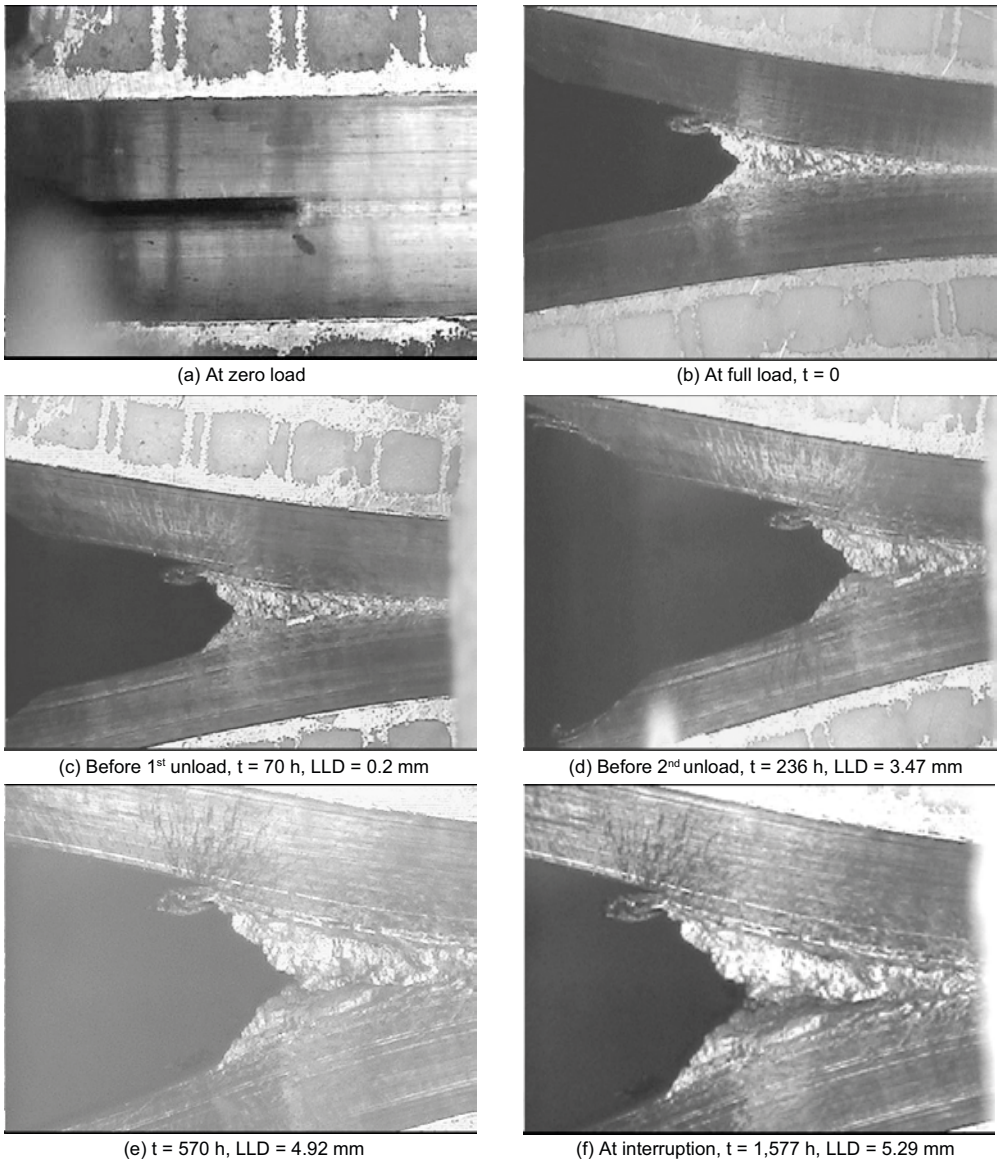

Figure 4-5. *Side view of notch tip opening at given time and corresponding LLD for the test at 125°C with side grooves. The distance between the lines in net is 2.5 mm.*

Figure 4-6 shows the side view of the crack tip for the test without side grooves. At the full load, the notch root radius had changed and two small cracks seem to have formed, see Figure 4-6(b). These two small cracks had apparently not developed at interruption when 2,256 hours had passed, see Figure 4-6(d).

4.2.3 CCG test using CT specimen without side grooves at 100°C/185 MPa

LLD and V/V_0 as a function of time are shown in Figure 4-7. LLD increased rapidly immediately after full loading. The increment of LLD slowed down gradually. At interruption at 2,925 hours, the LLD was 2.72 mm and the constant LLD rate approximately 0.03 μm/h. The V/V_0 recordings fluctuated and disturbances from the electrical supply system caused abrupt drops and jumps, see the blue line in Figure 4-7.

Figure 4-8 shows the side view of the crack tip. At the full load, the notch root radius was changed and small cracks seem to have been initiated, see Figure 4-8(b). Insignificant crack development was seen at interruption, see Figure 4-8(d).

4.2.4 CCG test using CT specimen without side grooves at 75°C/195 MPa

LLD and V/V_0 as a function of time are shown in Figure 4-9. LLD and V/V_0 behaved in a similar way to that for other CCG tests. Two load bar level readjustments, marked by [1] and [2], respectively, were made during the test. This led to a rapid increase in LLD immediately after the readjustments. At interruption, the LLD rate was 0.05 μm/h.

A CCG test at 75°C/165 MPa (Wu et al. 2013), see red line in Figure 4-9, is included for comparison. It is seen that the increase in reference stress from 165 MPa to 195 MPa caused larger LLD at the beginning of the test and somewhat higher LLD rate in spite of the fact that the previous test had side grooves.

Figure 4-10 exhibits the side view of crack tip, which is similar to that for other CCG tests. No crack growth is noticed.

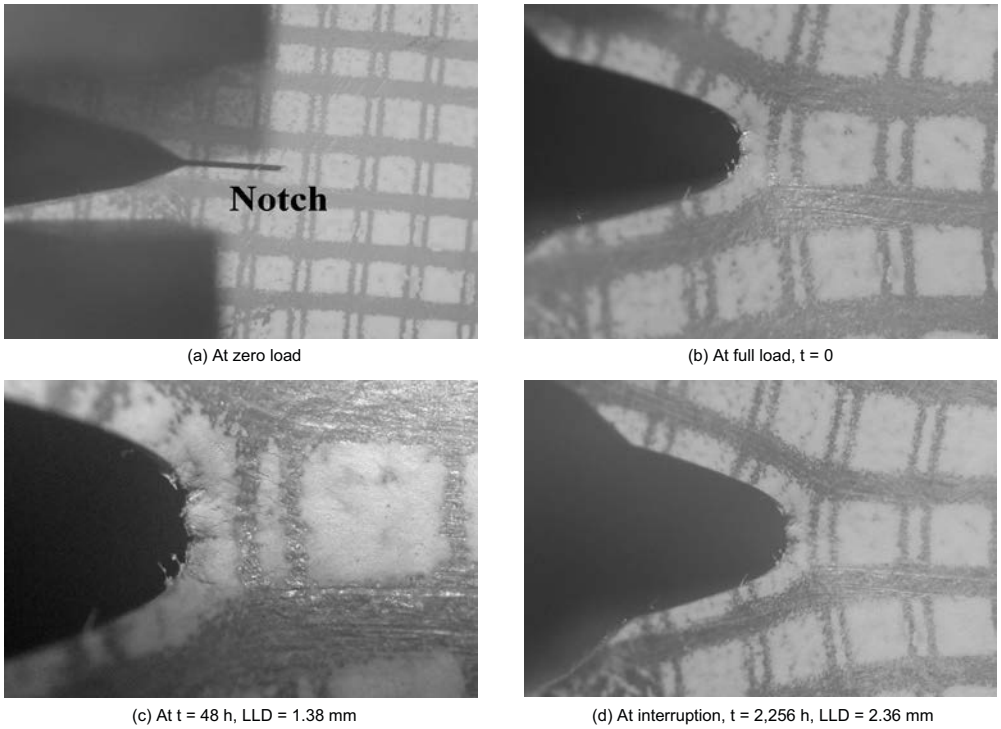

(a) At zero load

(b) At full load, t = 0

(c) At t = 48 h, LLD = 1.38 mm

(d) At interruption, t = 2,256 h, LLD = 2.36 mm

Figure 4-6. *Side view of notch tip opening at given time and corresponding LLD for the test at 125°C without side grooves. The distance between the lines in net is 2.5 mm.*

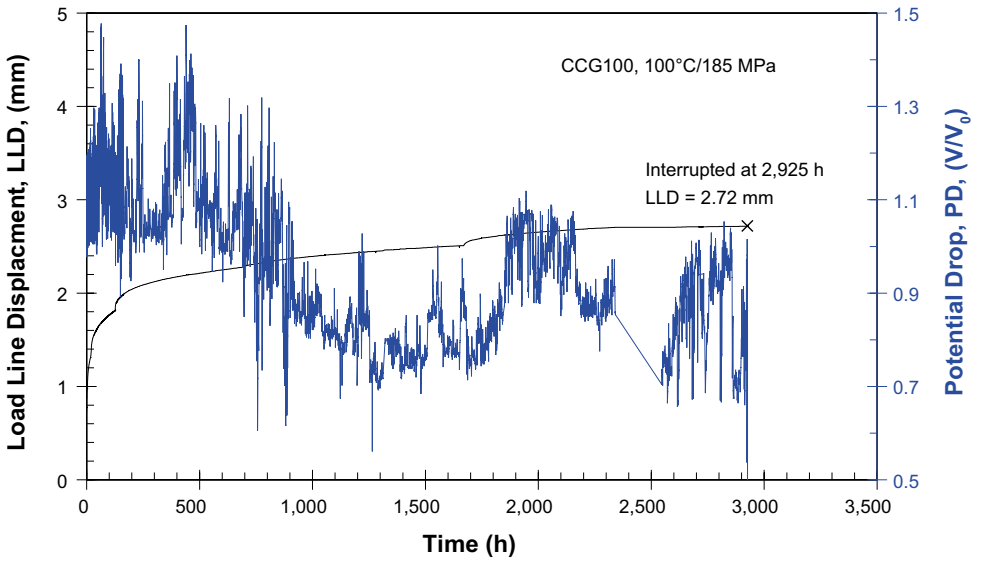

Figure 4-7. *Load line displacement (black line) and normalised potential drop (blue line) as a function of time for CCG test at 100°C/185 MPa. The test was interrupted at 2,925 h when LLD was 2.72 mm.*

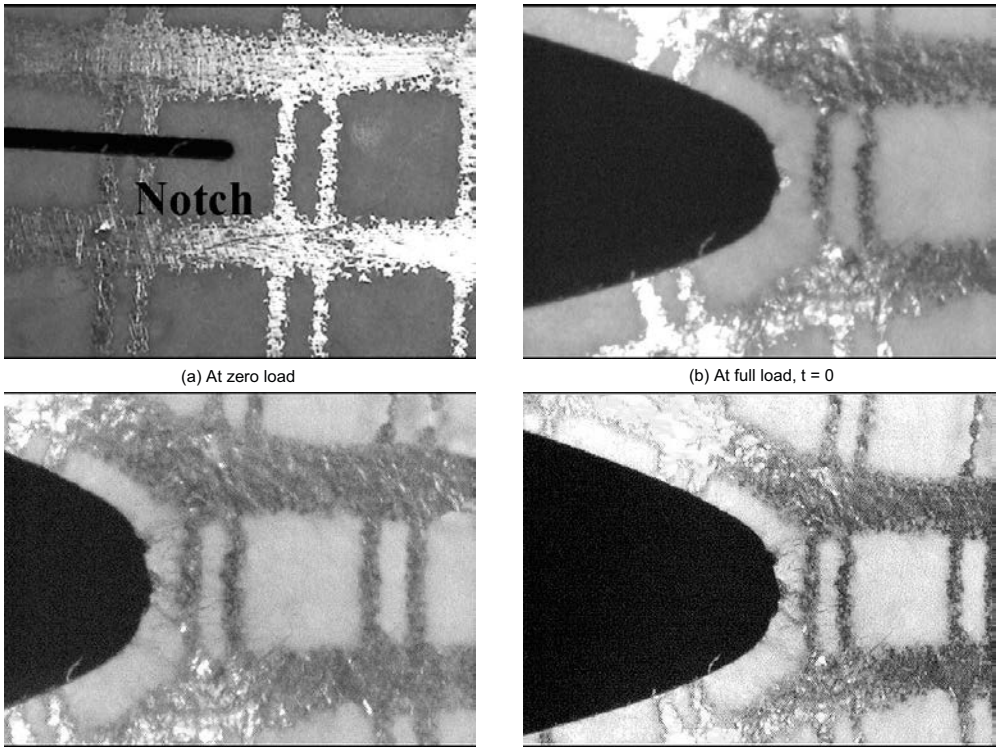

Figure 4-8. *Side view of notch tip opening at different times and corresponding LLD for the test at 100°C without side grooves. The distance between the lines in the net is 2.5 mm.*

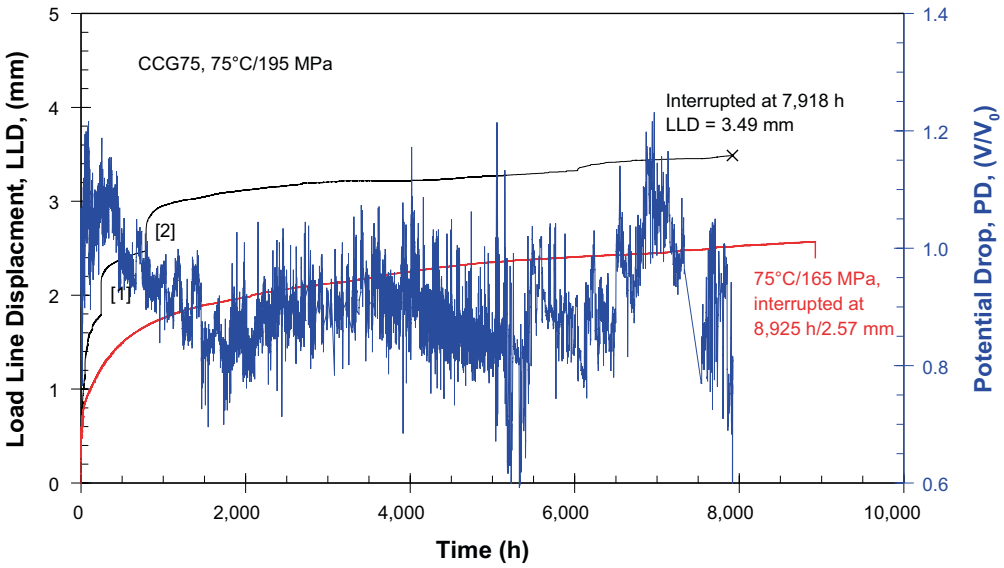

Figure 4-9. *Load line displacement (black line) and normalised potential drop (blue line) as a function of time for CCG test at 75°C/195 MPa. The test was interrupted at 7,918 h when LLD was 3.49 mm. An interrupted CCG test at 75°C/165 MPa with side grooves (red line) is included for comparison (Wu et al. 2013).*

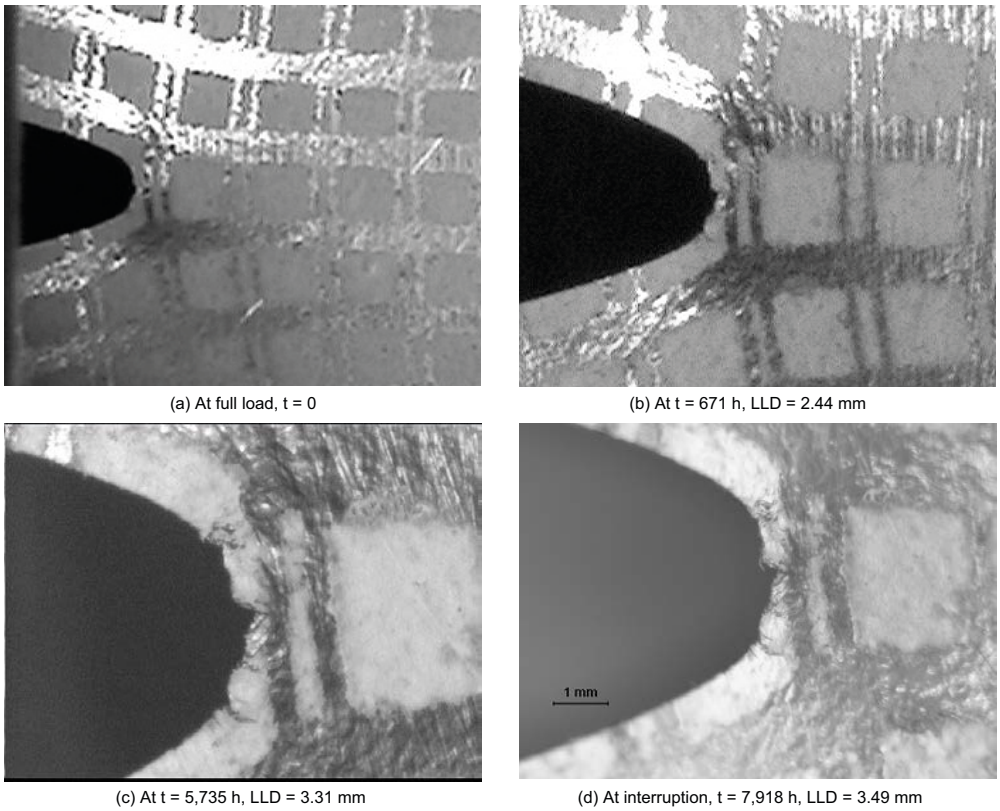

(a) At full load, t = 0

(b) At t = 671 h, LLD = 2.44 mm

(c) At t = 5,735 h, LLD = 3.31 mm

(d) At interruption, t = 7,918 h, LLD = 3.49 mm

Figure 4-10. *Side view of notch tip opening at given time and corresponding LLD for the test at 75°C without side grooves.*

4.3 Shear testing

Creep strain measured between the edges shown in Figure 3-6(a) is given as a function of time in Figure 4-11 for the two shear tests. The stress levels 75 and 80 MPa refer to average stresses across the specimen section. The applied load is consequently the stress multiplied by the size of the specimen cross section away from the notches. The test at 80 MPa failed and the test at 75 MPa was interrupted. It is unclear why strain immediately after start for the test at 80 MPa is lower than that for the test at 75 MPa. Nevertheless, the strain rate at 80 MPa was higher than that at 75 MPa, i.e. $3.60 \cdot 10^{-6}$/h and $3.69 \cdot 10^{-7}$/h, respectively.

It is seen that the test at 80 MPa undergoes primary, secondary and tertiary creep before it fails. The test at 75 MPa has entered secondary creep and it may have lasted long.

4.4 Compression testing

Creep strain as a function of time is given for compression tests generated for two material conditions, as-received and 24% cold worked, respectively, at 180 MPa and 75°C. All the tests were interrupted. After test, hardness was measured and is given in the figure. It is seen that all the tests have reached secondary creep. It is interesting to note that the two material conditions give about the same results.

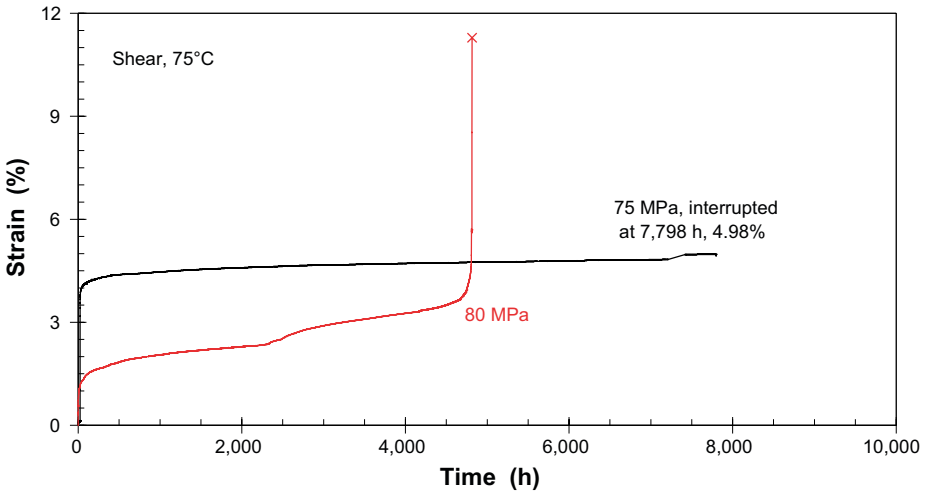

Figure 4-11. *Strain as a function of time for two shear tests at given stresses at 75°C. The test at 75 MPa was interrupted at 7,798 h with a strain of 4.98%.*

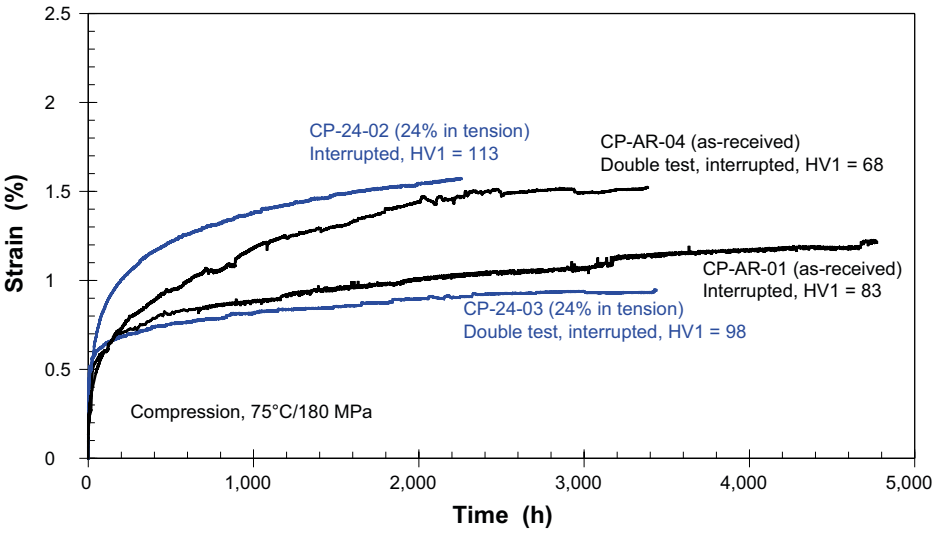

Figure 4-12. *Creep strain as a function of time for compression tests at 180 MPa and 75°C. Two material conditions were tested, as-received and 24% cold worked. All the tests were interrupted. After the tests, hardness was measured and its value is given in the figure. The text "double" in the graph indicates that it was the second test under the same conditions.*

5 Post test metallography

5.1 Metallographic study of CT specimens

5.1.1 CT specimen CCG175 without side grooves at 175°C/115 MPa

At interruption, the CT specimen CCG175 has been strongly bent, see Figure 5-1(a). Many small cracks have formed at the notch tip, Figure 5-1(b). This is consistent with the side view of the CT specimen CCG175, cf. Figure 4-3.

The CT specimen CCG175 has been sectioned in the middle and at sub-surface to investigate creep damage in front of the notch. At sub-surface, few cracks were observed to have initiated from the notch, see Figure 5-2(a). The cracks started to propagate intergranularly. Intergranular microcracks are also seen close to the notch tip, see Figure 5-2(b). In the middle, more creep cracks are seen to have formed and developed intergranularly, either from the notch or in front of the notch, see Figure 5-3. Creep cavities were observed 7 mm from the notch tip, see Figure 5-3(d).

Grains close to the notch were more strongly deformed in the middle than those at sub-surface, cf. Figure 5-2 and Figure 5-3.

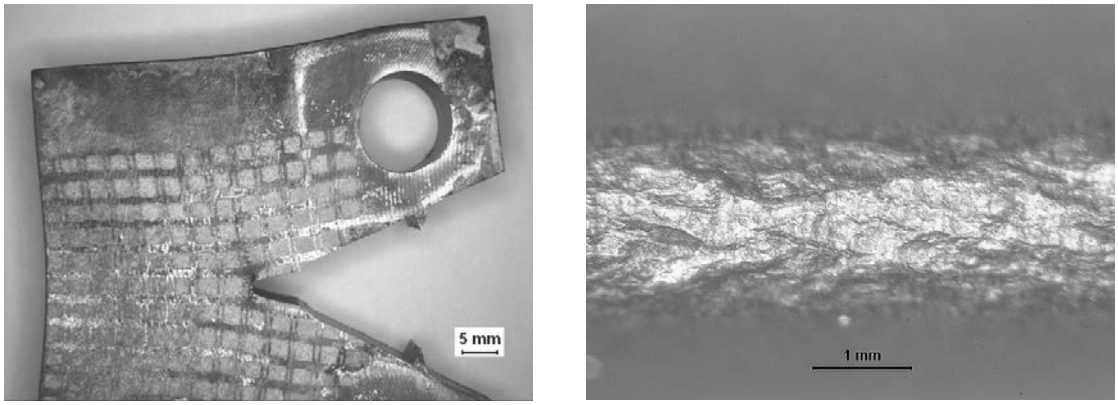

(a) Strongly bent CT specimen (a) Front view

Figure 5-1. *Specimen CCG175 at interruption. Side view is given in Figure 4-3.*

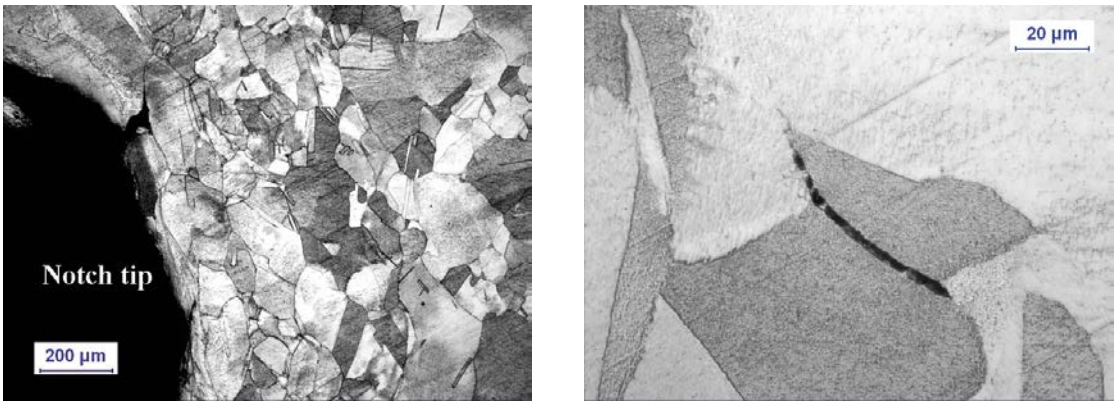

(a) Strongly deformed grains and microcracks close to the notch (a) Close to notch tip

Figure 5-2. *LOM images showing sub-surface of specimen CCG175. Creep cavities and microcracks are seen.*

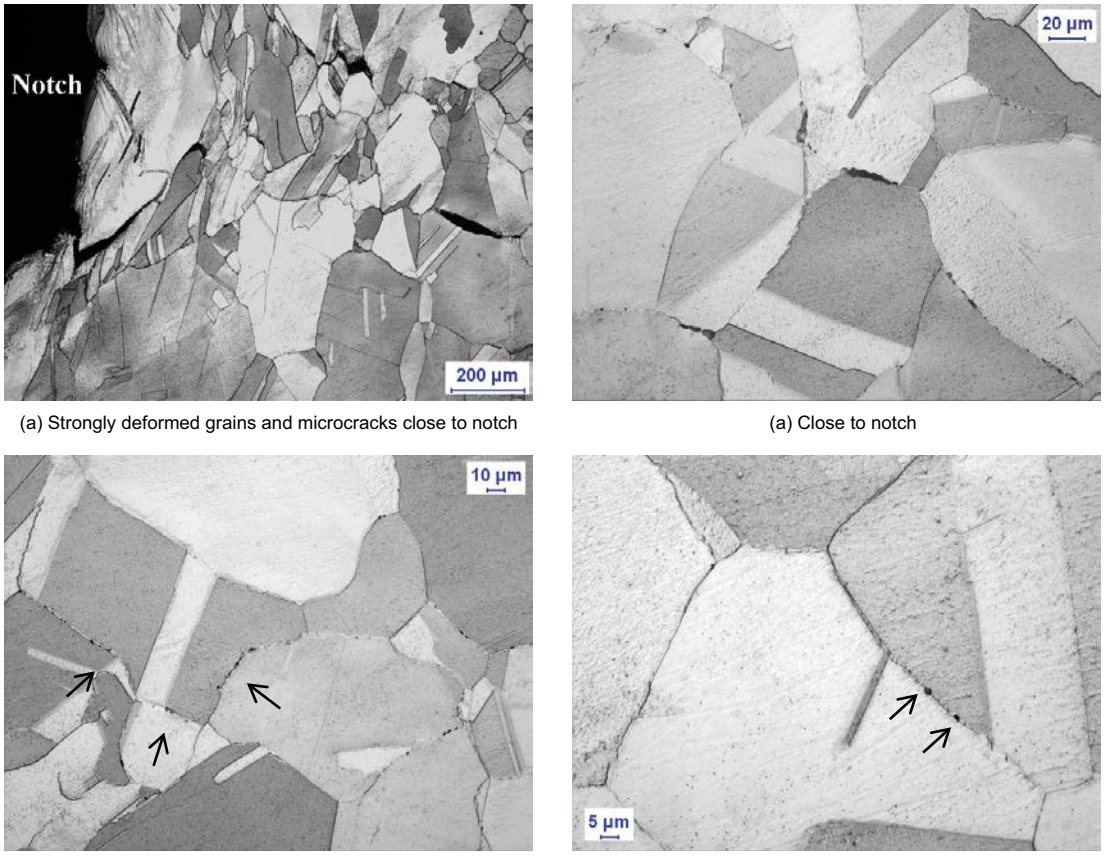

(a) Strongly deformed grains and microcracks close to notch

(a) Close to notch

(b) 3 mm from notch

(c) 7 mm from notch

Figure 5-3. *LOM images showing middle section of specimen CCG175. Creep cavities and cracks are seen. Arrow indicates some cavities.*

5.1.2 CT specimen CCG125-1 without side grooves at 125°C/165 MPa

The CT specimen CCG125-1 has been strongly bent at interruption, see Figure 5-4(a). Many small shallow cracks were formed at the notch tip, Figure 5-4(b). This is verified by the side view of the CT specimen CCG125-1, cf. Figure 4-6.

The CT specimen CCG125-1 was sectioned in the middle and at sub-surface. At sub-surface, only strongly deformed grains are visible, see Figure 5-5. In the middle, a few creep cavities and cracks had formed and developed intergranularly, either from the notch or in front of the notch, see Figure 5-6. Creep cavities are observed 5 mm from the notch tip, see Figure 5-6(d).

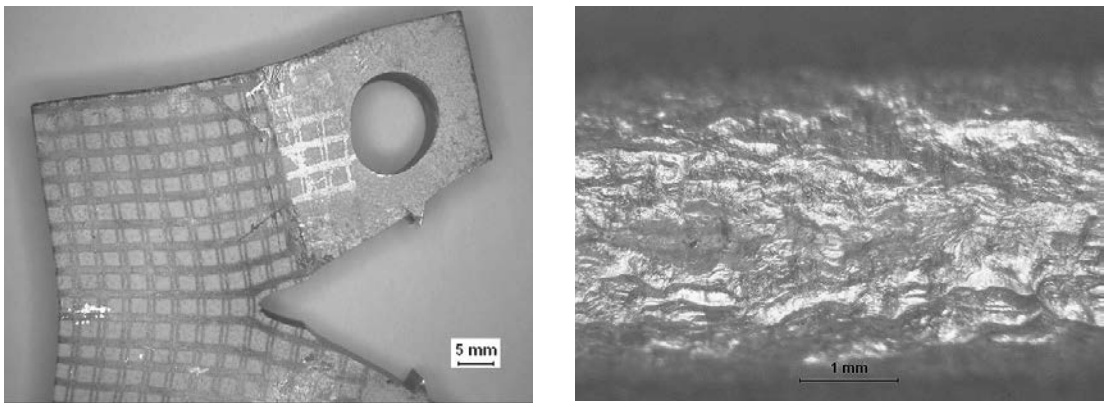

(a) Strongly bent CT specimen

(b) Front view

Figure 5-4. *Specimen CCG125-1 at interruption. Side view is given in Figure 4-6.*

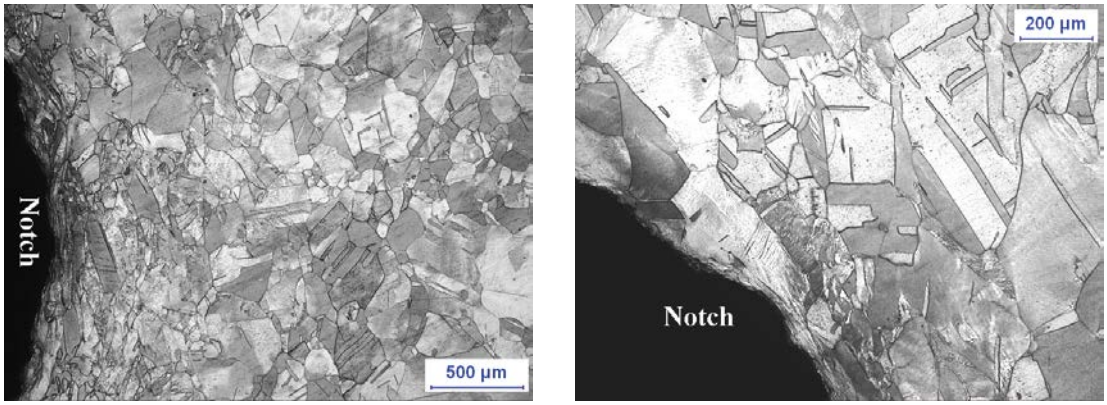

(a) Strongly deformed grains close to notch (b) Strongly deformed grains close to notch

Figure 5-5. *LOM images showing sub-surface of specimen CCG125-1. Strongly deformed grains close to notch.*

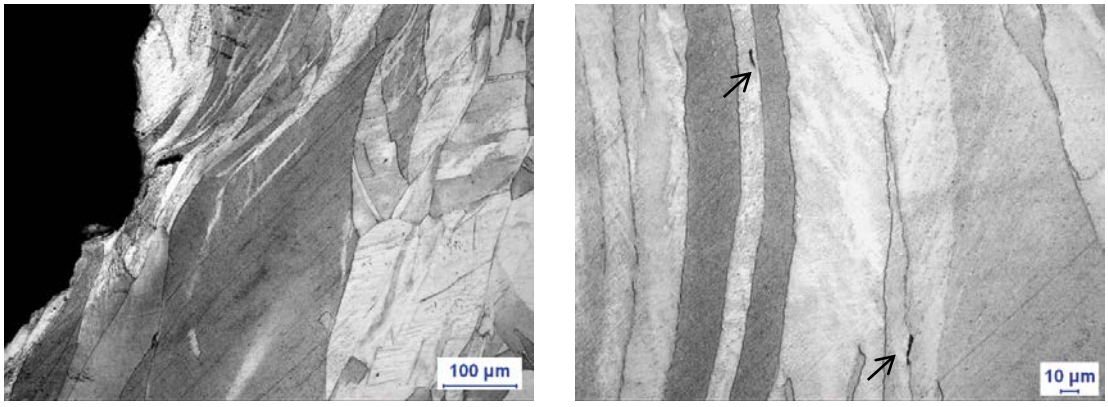

(a) Strongly deformed grains and microcrack close to notch (b) Adjacent to notch

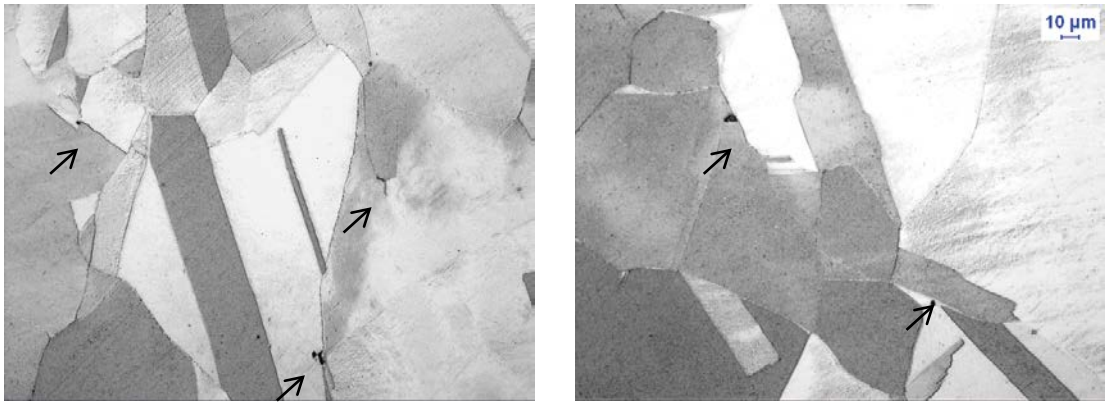

(c) 1 mm from notch (d) 5 mm from notch

Figure 5-6. *LOM images showing middle section of specimen CCG125-1. Creep cavities and cracks are seen. Arrows indicate cavities.*

5.1.3 CT specimen CCG125-2 with side grooves at 125°C/170 MPa

The CT specimen CCG125-2 was strongly bent at interruption in the same way as specimens without side grooves, see Figure 5-7(a). Due to extraordinarily large crack opening, the extensometer attached to the knife edge of the CT specimen detached, see arrows in Figure 5-7(a). This will give wrong LLD measurements. Significant crack formation and growth have been found on the side grooves, see Figure 5-7(b)–(d) and Figure 4-5. Separated surfaces due to crack growth have been heavily oxidised, implying that crack growth has happened for a long period.

The CT specimen CCG125-2 was sectioned in the middle and at sub-surface. At sub-surface, strongly deformed grains and microcracks to a small extent were visible, see Figure 5-8. In the middle, strongly deformed grains and extensive intergranular creep cavities and cracks were found close to the notch, see Figure 5-9. Creep cavities were observed 10 mm from the notch tip, see Figure 5-9(d).

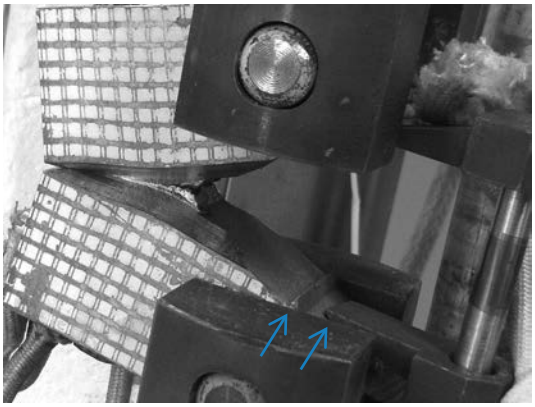

(a) At interruption. Extensometer has detached from the knife edge of the strongly bent CT specimen, indicated by arrows

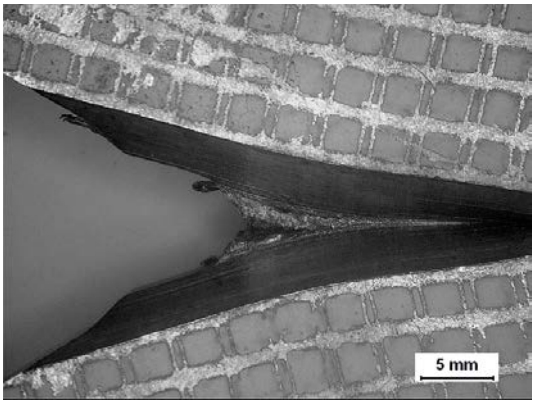

(b) Side view, see also Figure 4-5

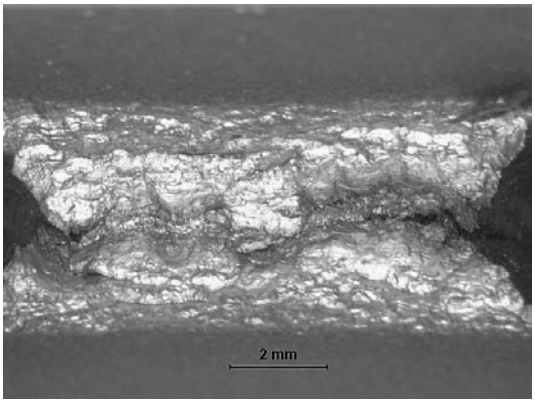

(c) Front view. Cracks at side groove

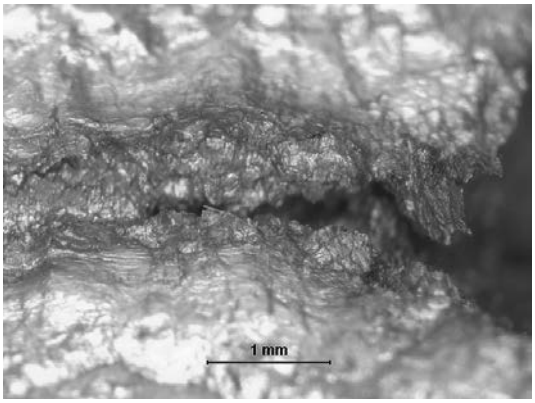

(d) Same as (c), but higher magnification

Figure 5-7. *Specimen CCG125-2 at interruption. Side view is also given in Figure 4-5.*

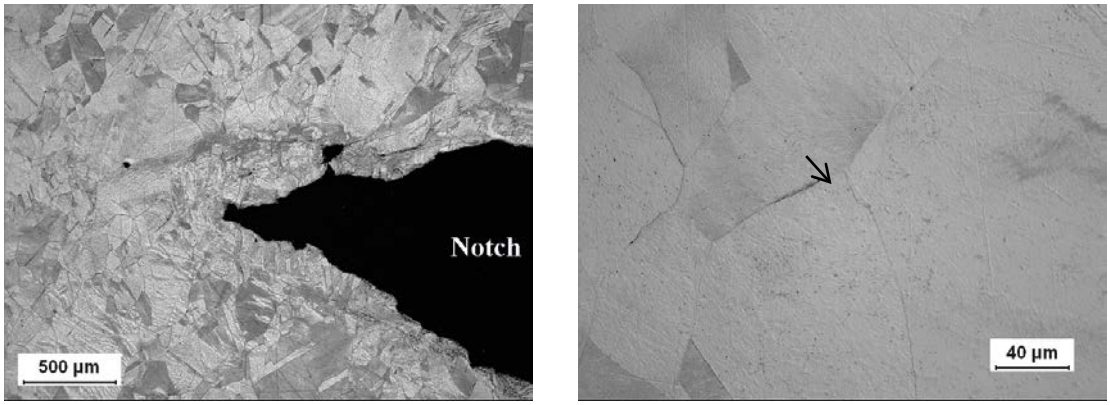

(a) Strongly deformed grainsclose to notch and crack growth from notch

(b) Intergranular crack

Figure 5-8. *LOM images showing sub-surface of specimen CCG125-2. Strongly deformed grains and microcracks close to notch.*

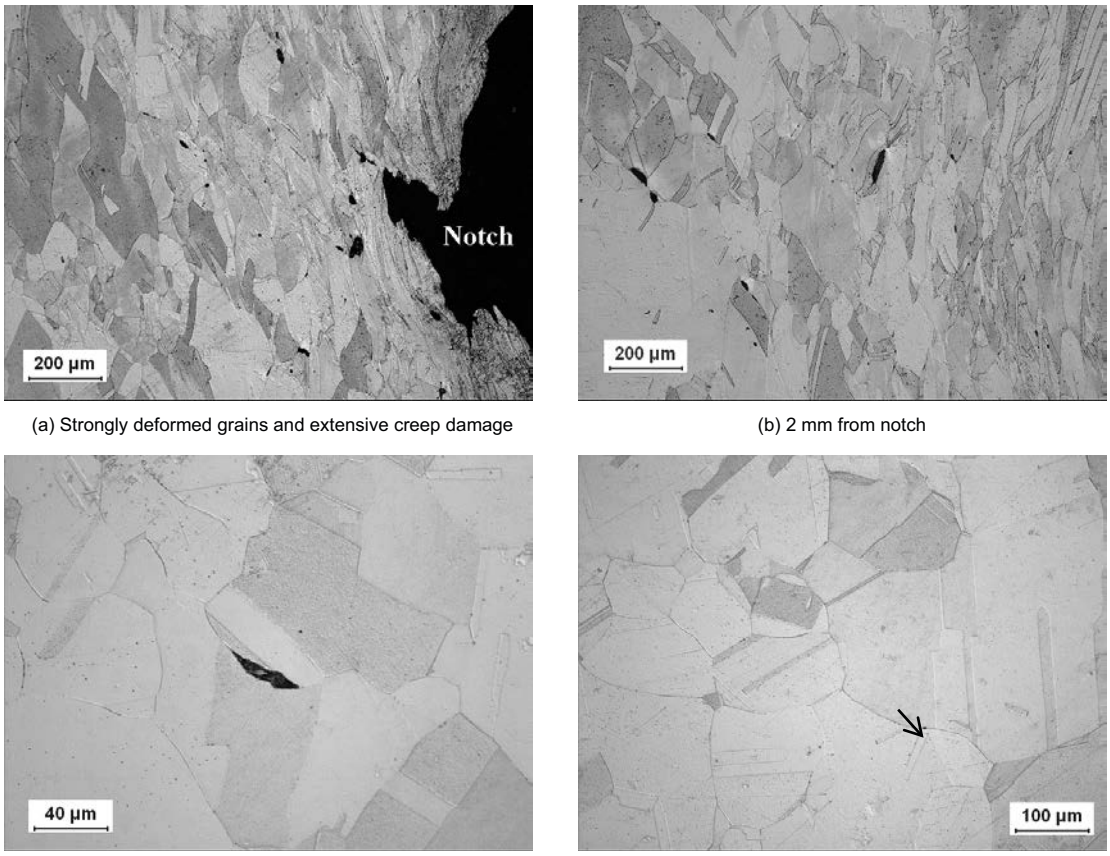

(a) Strongly deformed grains and extensive creep damage

(b) 2 mm from notch

(c) 7 mm from notch

(d) 10 mm from notch

Figure 5-9. *LOM images showing middle section of specimen CCG125-2. Intergranular creep cavities and cracks are found. Arrow indicates cavities.*

5.1.4 CT specimen CCG100 without side grooves at 100°C/185 MPa

The CT specimen CCG100 has been strongly bent at interruption, see Figure 5-10(a). Few small shallow cracks had formed at the notch tip, Figure 5-10(b). This is consistent with the side view observation, cf. Figure 4-8. Grains close to the notch were strongly deformed at sub-surface and in the middle, see Figure 5-11(a) and (b), respectively. No creep damage was observed at sub-surface. Creep cavities to limited extent were found in the middle and also at 2 mm from the notch, see Figure 5-11(c) and (d).

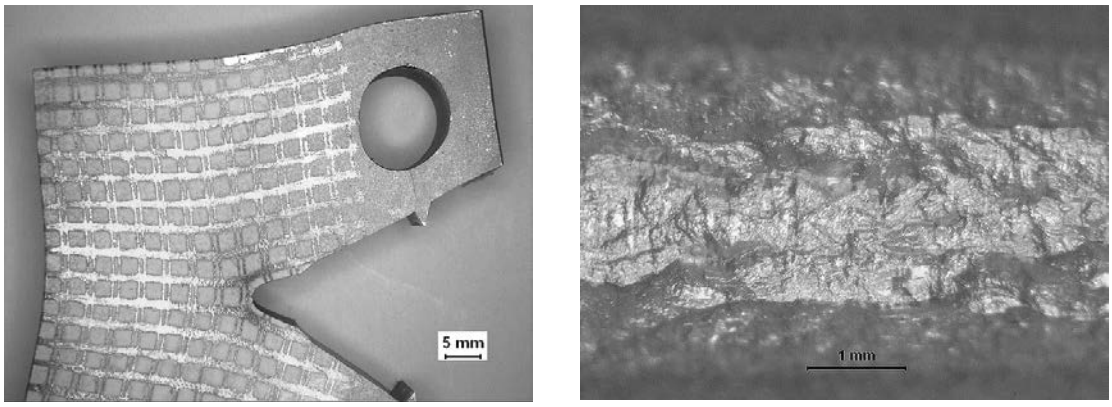

(a) Strongly bent CT specimen (b) Front view

Figure 5-10. *Specimen CCG100 at interruption. Side view is given in Figure 4-8.*

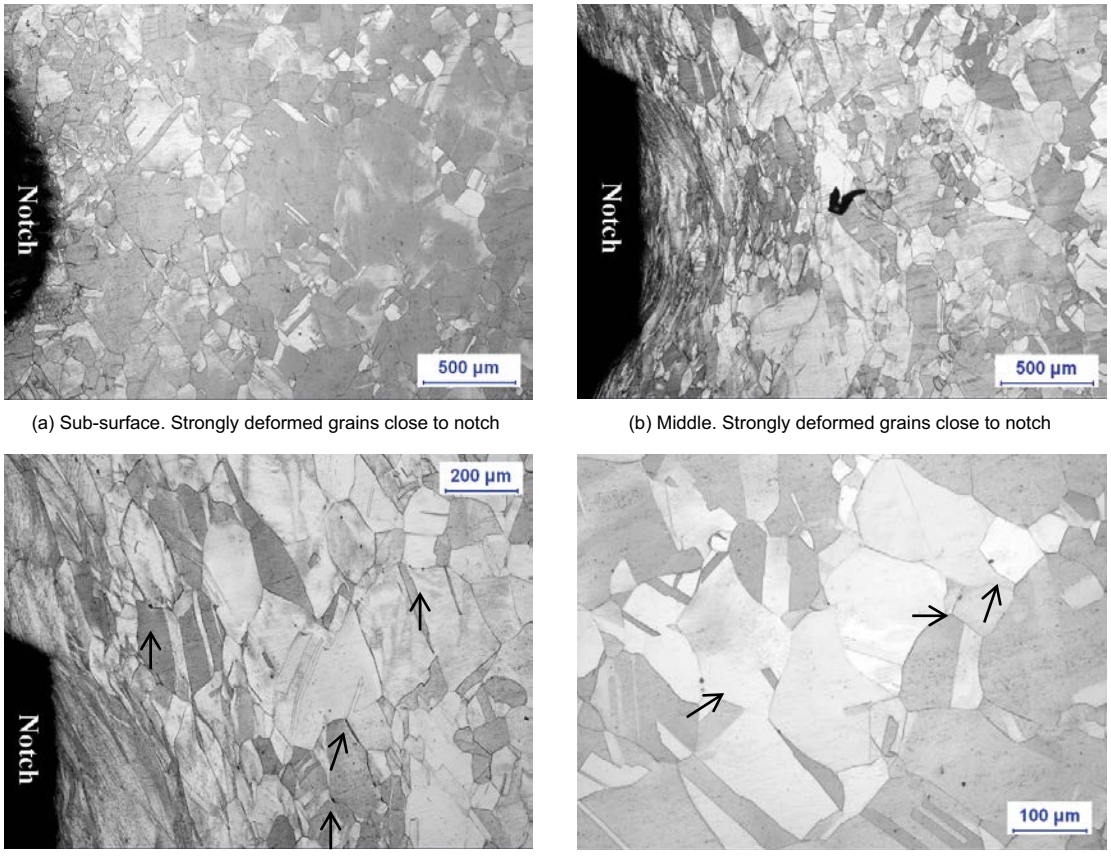

(a) Sub-surface. Strongly deformed grains close to notch

(b) Middle. Strongly deformed grains close to notch

(c) Middle. Strongly deformed grains and creep cavities

(d) Middle. 2 mm from notch

Figure 5-11. *LOM images showing sub-surface as well as middle section of specimen CCG100. Intergranular creep cavities and cracks were found in the middle section, indicated by arrow.*

5.1.5 CT specimen CCG75 without side grooves at 75°C/195 MPa

The specimen CCG75 was also strongly deformed at interruption, see Figure 5-12(a). Few small shallow cracks had formed at the notch tip, Figure 5-12(b) and Figure 4-8. Grains close to the notch were strongly deformed at sub-surface and in the middle, see Figure 5-13(a) and (b), respectively. No creep damage has been observed at sub-surface. Creep cavities to a small extent were found in the middle section and also at 1 mm from the notch, see Figure 5-13(c) and (d).

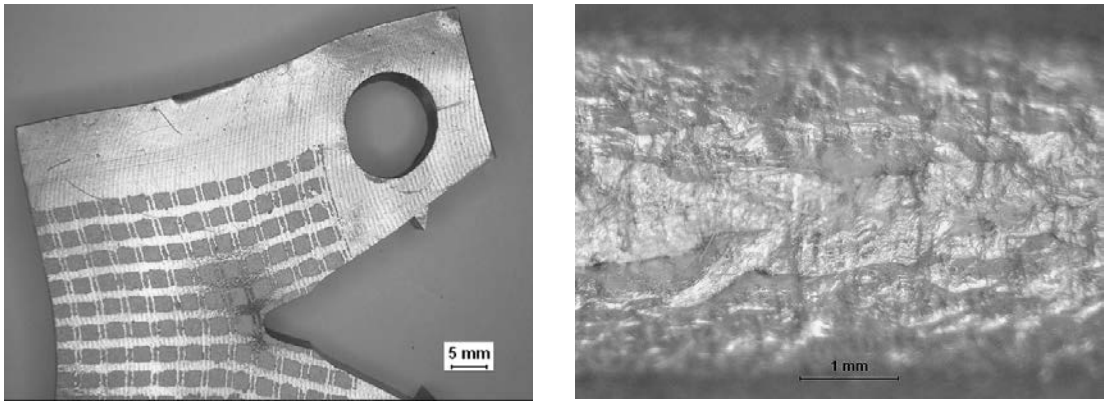

(a) Strongly bent CT specimen (b) Front view

Figure 5-12. *Specimen CCG75 at interruption. Side view is given in Figure 4-10.*

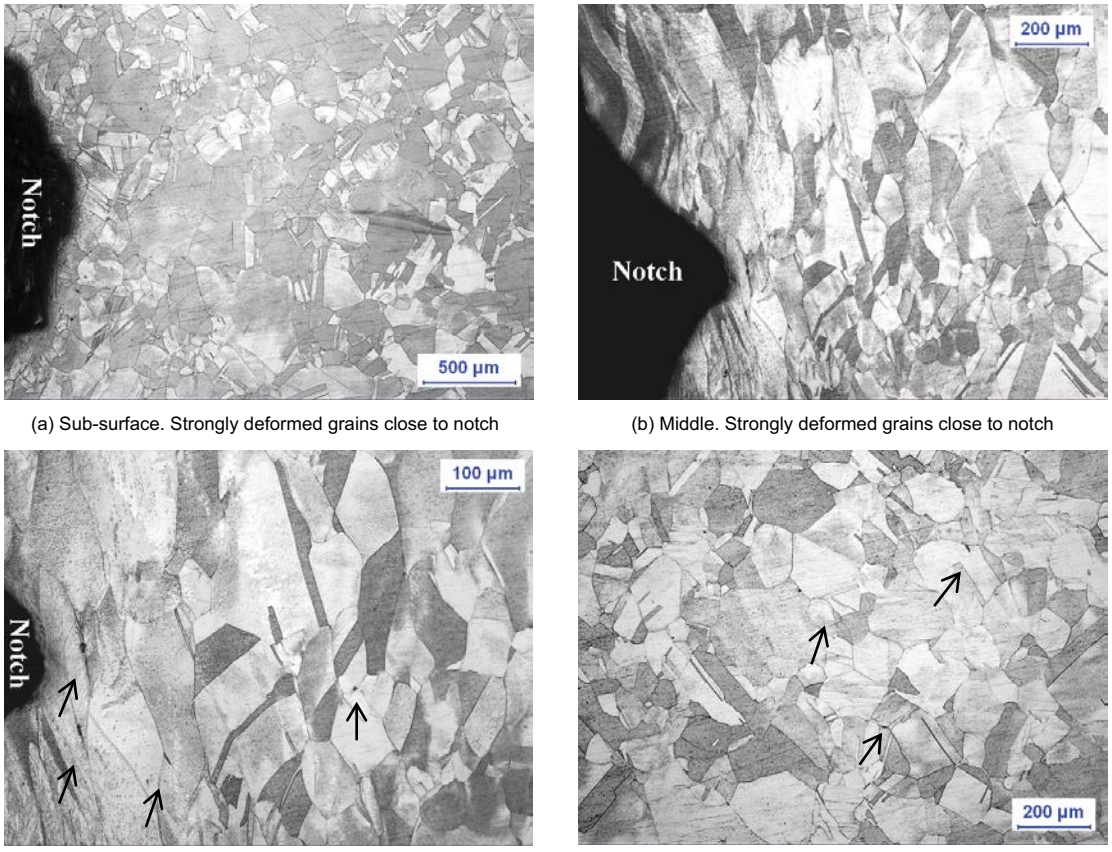

(a) Sub-surface. Strongly deformed grains close to notch (b) Middle. Strongly deformed grains close to notch

(c) Middle. Strongly deformed grains and creep cavities (d) Middle. 1mm from notch

Figure 5-13. *LOM images showing sub-surface as well as middle section of specimen CCG75. Intergranular creep cavities and cracks were found in the middle section, indicated by arrows.*

5.2 Plate shear specimen

Images taken during the test and at rupture are shown in Figure 5-14 for the test at 75°C/80 MPa. It can be seen that notch acuity was altered at full load, cf. Figure 3-6 and Figure 5-14(a). Strong deformation was observed to concentrate at two places which were some distance from the notch tip, see arrow in Figure 5-14. Cracks initiated from these two places simultaneously, see Figure 5-14(b)–(d). Meantime, the specimens were sheared so that the vertical lines of the measuring net were twisted. Two main cracks, one developed from each notch at the very end of the test, propagated vertically to the applied stress direction and caused final rupture, see Figure 5-14(e)–(f).

Images taken during the test and at interruption are shown in Figure 5-15 for the test at 75°C/75 MPa. Notch acuity was slightly altered at full load, cf. Figure 3-6 and Figure 5-15(a). At beginning of the test, the specimen deformed rapidly and strongly, which led to an obvious opening of the notches, see Figure 4-10, Figure 5-15(a) and (b). As the test continued, strain accumulation slowed down to a constant rate of $3.69 \cdot 10^{-7}$/h. Opening of the notches was not as obvious as that in the beginning of the test, see Figure 5-15(c) and (d). There were no measureable cracks formed.

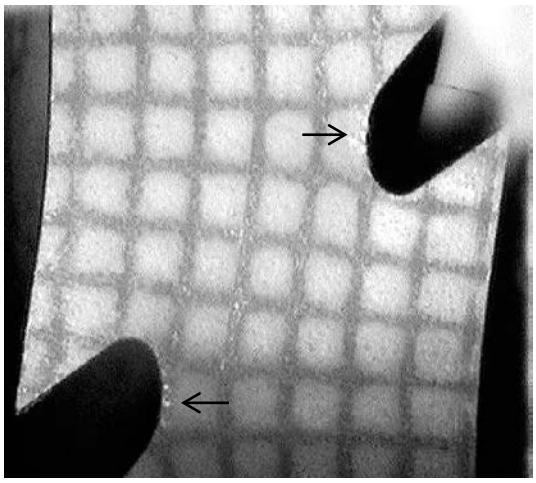

(a) At full load, t = 0

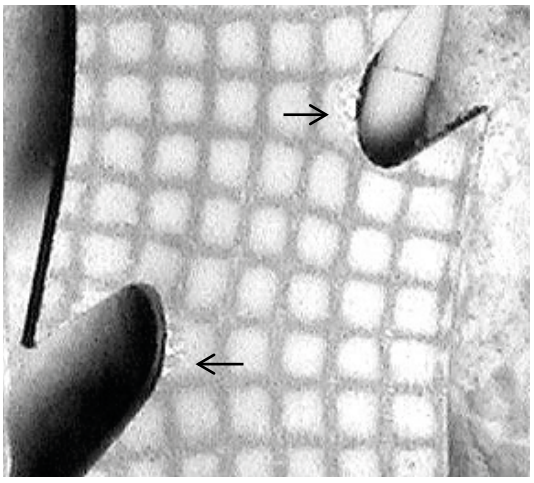

(b) Att = 113 h, ε = 1.49%

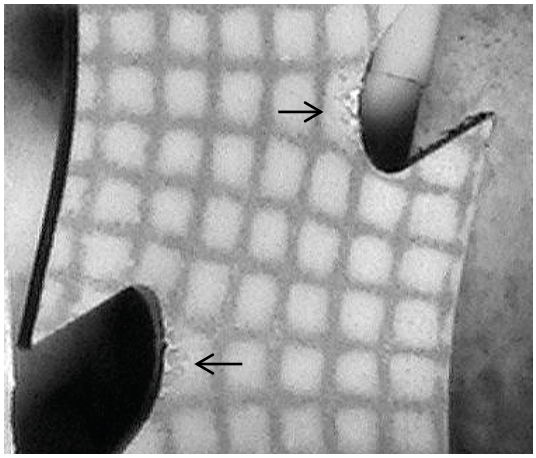

(c) At t = 2,687 h, ε = 2.72%

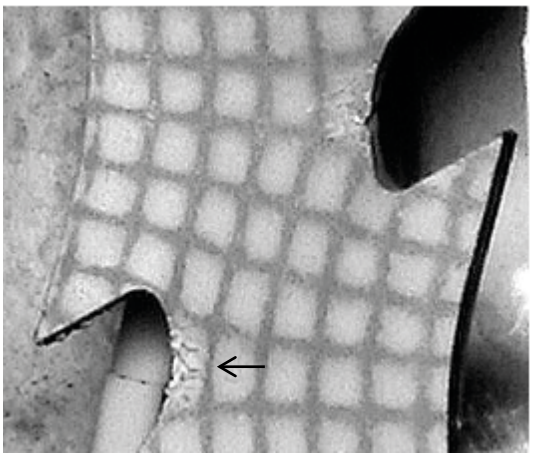

(d) At t = 4,700 h, ε = 3.76%

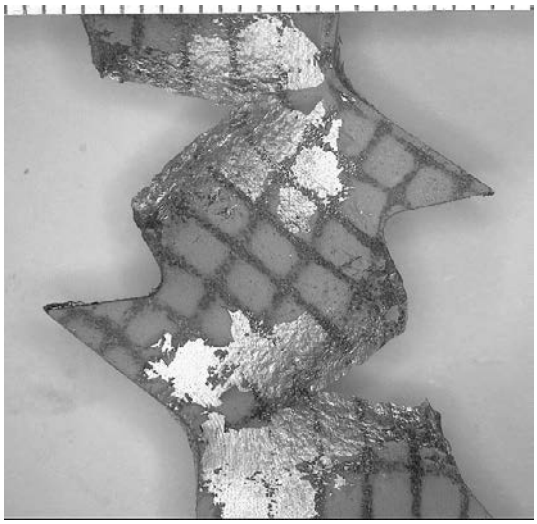

(e) At rupture t = 4,814 h, ε = 11.3%

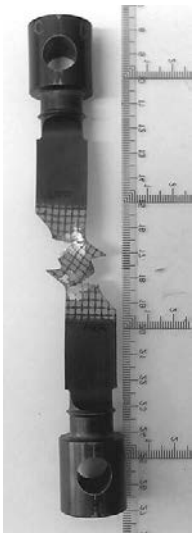

(f) At rupture t = 4,814 h, ε = 11.3%

Figure 5-14. *Side view of opening of 45° notches at given time and strain for the shear test at 75°C/80 MPa. The shear specimen prior to the test is shown in Figure 3-6. Arrow indicates where strong deformation occurred and where cracks initiated and grew.*

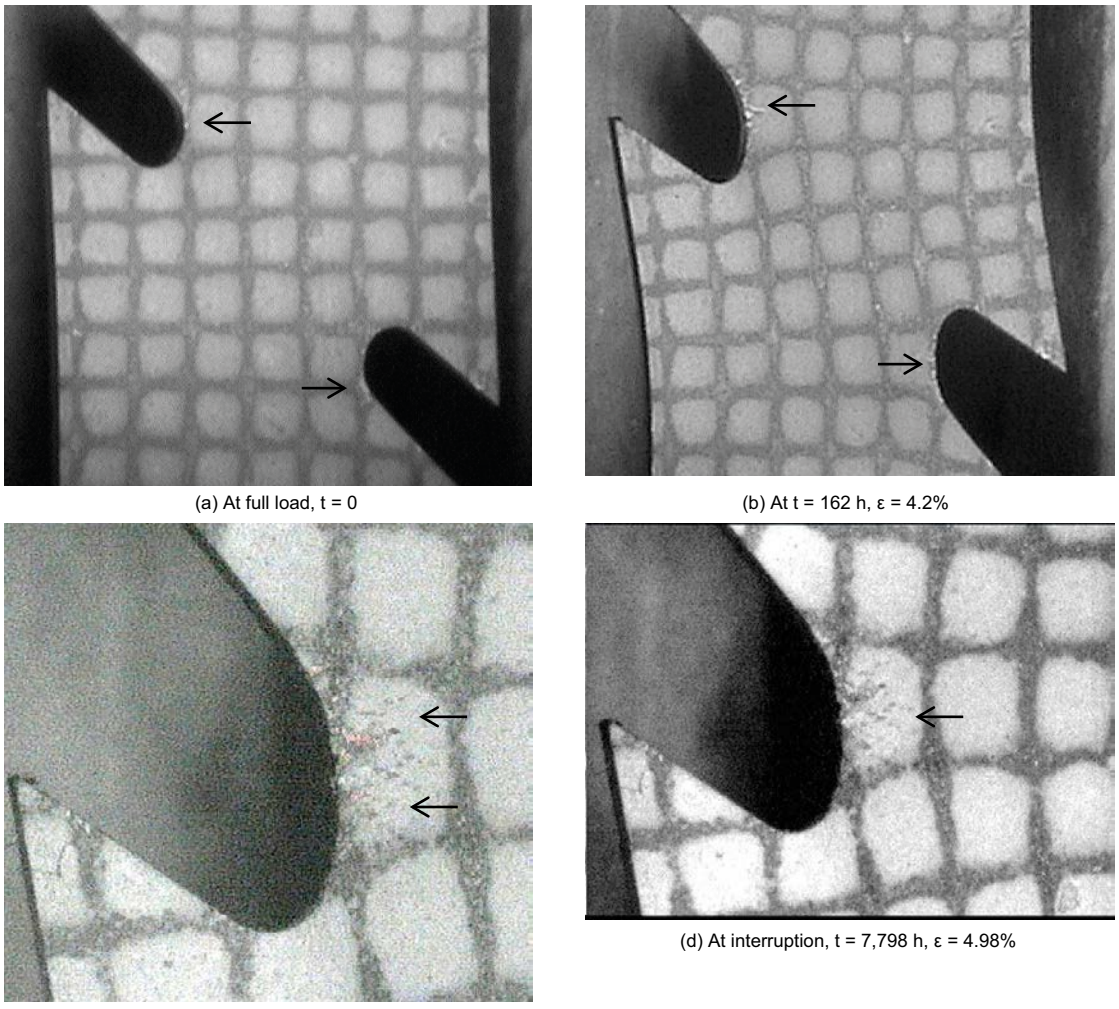

(a) At full load, t = 0

(b) At t = 162 h, ε = 4.2%

(c) At t = 5,612 h, ε = 4.77%

(d) At interruption, t = 7,798 h, ε = 4.98%

Figure 5-15. *Side view of opening of 45° notches at given time and strain for the shear test at 75°C/75 MPa. The test is interrupted at 7,798 hours and 4.98%. The shear specimen prior to the test is shown in Figure 3-6. Arrow indicates where strong deformation occurred and where cracks may have initiated.*

6 Modelling and discussion

6.1 Cold worked notched specimens

The creep strain curves for the notched round creep specimens were given in Figure 4-1. The life of these specimens is compared with previously performed tests in Figure 6-1.

Uniaxial results for as-received Cu-OFP are taken from Andersson et al. (2007), uniaxial results for 24% cold worked Cu-OFP from Wu et al. (2014), and results for notched specimens for as-received material for notch acuity of 5 from Wu et al. (2009b). These results are compared with those from the present investigation for notched specimens for cold worked Cu-OFP. The figure demonstrates for the as-received material that the effect of multiaxiality can be taken into account by making the comparison for a given reference stress (Wu et al. 2009b). The relation between the net section σ_{net} and the reference stress σ_{ref} can be expressed as

$$\sigma_{ref} = \sigma_{net} / f_{ref} \qquad \text{(Equation 6-1)}$$

For a notch acuity of 5, the factor f_{ref} is 1.328 (Wu et al. 2009b). After 24% cold work in tension, the creep rupture strength is considerably raised. In fact the rupture strength is about 30% higher at 75°C (Wu et al. 2014). The notched and cold worked specimens with the highest stress have a reference stress which is about that for cold worked material without notches. This shows that the notched and cold worked Cu-OFP is at least as strong as the reference stress suggests.

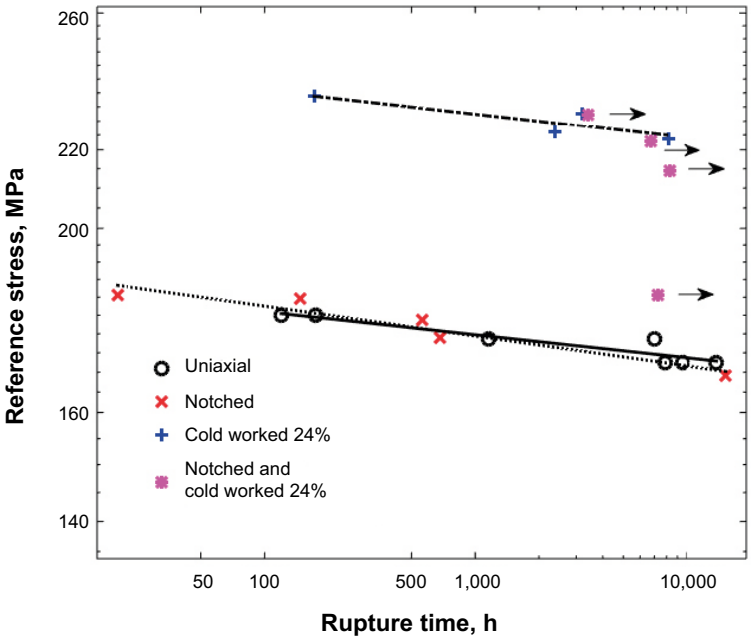

Figure 6-1. *Reference stress versus rupture time for four groups of specimens i) uniaxial, ii) notched but not cold worked; iii) cold worked but not notched and iv) notched and cold worked. Arrows indicate interrupted tests. Lines are fitted to three of the data sets to increase the visibility.*

6.2 Modelling of crack propagation in CT specimens

A model for crack propagation in Cu-OFP has recently been presented (Wu et al. 2013). This is based on creep damage development in front of the crack in the form of cavitation. When the cavitated fraction in the grain boundaries exceeds a certain value (25%), the crack is assumed to propagate. The details of the model are fully described in the published paper and are not repeated here.

In the publication the model was applied to CT specimens with side grooves tested at 20, 75, 175 and 215°C. Two of the specimens tested at 175 and 215°C ruptured. The other specimens tested at 20 and 75°C did not show any crack propagation. The results are included in Table 6-2 (see below).

In the present investigation four out of five specimens did not have any side grooves. This affects the multiaxial stress state in front of the crack. The cavity growth rate is proportional to the stress perpendicular to the crack front σ_1 (the largest principal stress) and a factor g_{multi} that depends on the ratio between the hydrostatic stress σ_m and the effective stress σ_{eff}.

$$g_{\text{multi}} = e^{\left(\frac{3\sigma_m}{2\sigma_{eff}} - \frac{1}{2}\right)} \qquad \text{(Equation 6-2)}$$

The appropriate stress ratios are listed in Table 6-1. The values are taken from the FEM stress analysis just in front of the crack (≤ 0.2 mm). These values have the largest influence on the crack propagation.

For the specimens without side grooves tested at 75, 100, 125 and 175°C the model does not give any crack propagation. This is in full agreement with the observations, see Table 6-2.

The predicted creep damage for the specimen with side grooves tested at 125°C is illustrated in Figure 6-2. This illustrates brittle creep which cavities only near the crack tip. However, ductile tearing can also give rise to cavity formation due to the large deformation in the specimens. This is probably the reason for the cavities that are found in front of the crack tip. For a further discussion of such cavities, see Wu et al. (2013). Ductile tearing is taken into account in the crack propagation model.

Table 6-1. Values for multiaxial stress parameters in front of the crack.

Parameter	With side growths	Without side grooves
σ_m/σ_{eff}.	13.5	7.2
σ_1/σ_{eff}.	7.45	2.99

Table 6-2. Modelled crack propagation results.

Specimen designation	Temperature (°C)	Reference Stress (MPa)	Time at interruption, (h)	Approx. observed crack propagation, mm	Modelled crack propagation, mm	Reference
CCG175NSG	175	115	12,286	0	0	1
CCG125-1NSG	125	165	2,256	0	0	1
CCG125-2SG	125	170	1,577	0.5	0.3	1
CCG100NSG	100	185	2,925	0	0	1
CCG75NSG	75	195	7,918	0	0	1
CCG215	215	130.2	121*	10	14	2
CCG175	175	132.7	812*	10	11	2
CCG75A	75	179.1	8,925	0	0	2
CCG75R	75	150.6–177.5	4,778	0	0	2
CCG22	22	146.9–222.2	13,324	0	0	2

References: 1. Present work; 2: Wu et al. (2013).

* Ruptured.

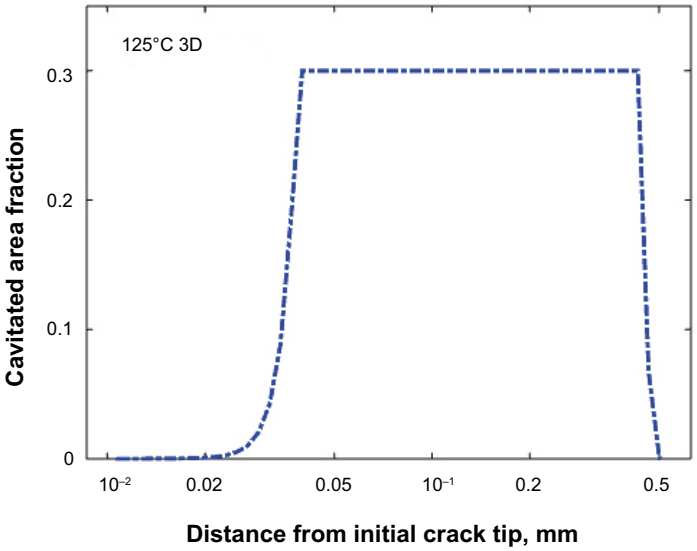

Figure 6-2. *Predicted amount of creep damage expressed as fraction of cavitated grain boundary area in front of the crack tip at interruption. 3D indicates that the specimen has side grooves. Simulated specimen CCG125-2SG.*

The predicted crack propagation as a function of time is shown in Figure 6-3.

The test was interrupted after 1,577 h, which gives a predicted crack propagation of 0.3 mm. The observed crack propagation was about 0.5 mm. In the experiments the crack appeared after about 100 to 200 h, see Figure 4-5. This in good agreement with the computations where the crack is found after about 200 h.

From the results from this and the previous investigation it can be concluded that the model can predict when significant crack propagation takes place, but the observed crack length cannot always be computed precisely. The model can clearly describe the role of the side grooves. Significant crack propagation has not been observed without the presence of side grooves. This indicates that highly constrained notches more readily develop into cracks.

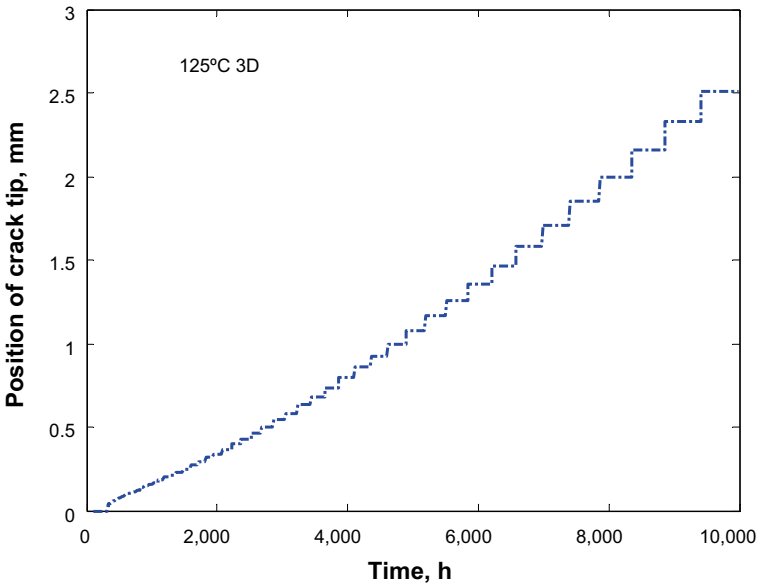

Figure 6-3. *Predicted crack tip position versus testing time specimen CCG125-2SG.*

6.3 Plate shear specimen

The stress and strain distributions in the shear specimens have been simulated with the help of FEM software (Comsol) in an elasto-plastic calculation. The von Mises stress distribution around the notches is shown in Figure 6-4 for the specimen tested at 80 MPa. The highest stresses lie in a band between the notches. In this band the stress is between 180 and 190 MPa. The distribution of stresses above 150 MPa is fairly complex almost in the shape of a Z. This is probably the main reason for the complicated nature of the failure, cf. Figure 5-14.

The plastic strain distribution corresponding to that in Figure 6-4 is shown in Figure 6-5. Again a band of high strains is observed between the notches. The highest strains are found at the right most and leftmost position of the notches. This is precisely where the deformation is located in the creep tested specimens, Figure 5-14 and Figure 5-15.

It is possible to obtain the failure stress of specimens exposed to a multiaxial stress state by using the reference stress method (Webster and Ainsworth 1994). If the creep exponent is very large, the stress field giving stationary creep deformation is the same as that at plastic collapse for a rigid plastic solid, but with the reference stress σ_{ref} instead of the yield strength σ_y.

$$P = \frac{P_L}{\sigma_y}\sigma_{\text{ref}} \qquad \text{(Equation 6-3)}$$

P is the applied load and P_L is the limit load (collapse load) for a rigid plastic material with a given yield strength. σ_{ref} is in this case the stress far from the notches. The chosen yield strength is the highest stress in the material. No plastic deformation is allowed and the stress analysis is elastic. If the stress exceeds the yield strength the component fails. The limit load has been reached. When the specimen is approaching the limit load, a band of fully yielded material across the specimen appears. The specimen with the stress 80 MPa far from the notches is taken as an example. The plastic flow stress (yield strength) is the uniaxial rupture strength at the lifetime of the specimen 4,814 h, which is 173 MPa (Andersson et al. 2007). With an average applied stress of 80 MPa on the specimen the resulting von Mises stress distribution is shown in Figure 6-6. The figure clearly demonstrates that the conditions correspond to the collapse load. Since the creep exponent is very high $n = 65$ at 75°C, the reference stress method should give an accurate result.

From Figure 6-5, it can be seen that the local strain is high at the notches (> 35%). This does not prevent that the rupture strength can be predicted with the reference stress method.

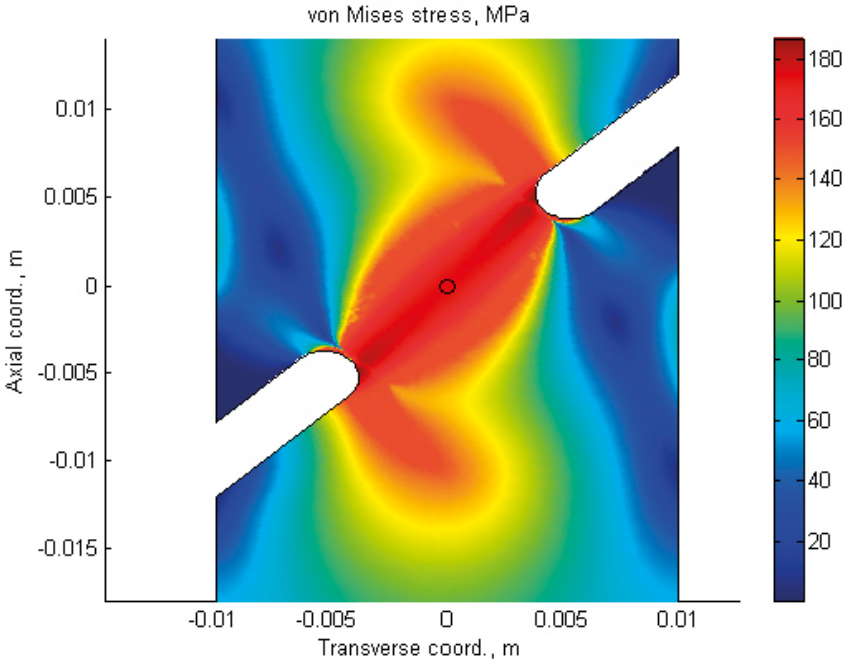

Figure 6-4. *von Mises stress distribution around the notches for the shear specimen tested at 75°C and 80 MPa.*

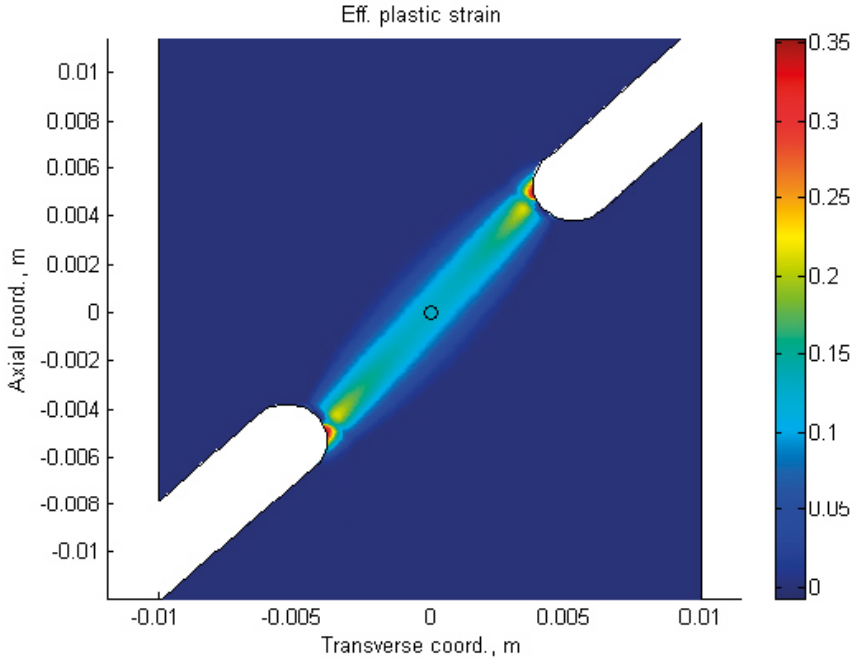

Figure 6-5. *Plastic strain distribution around the notches for the shear specimen tested at 75°C and 80 MPa.*

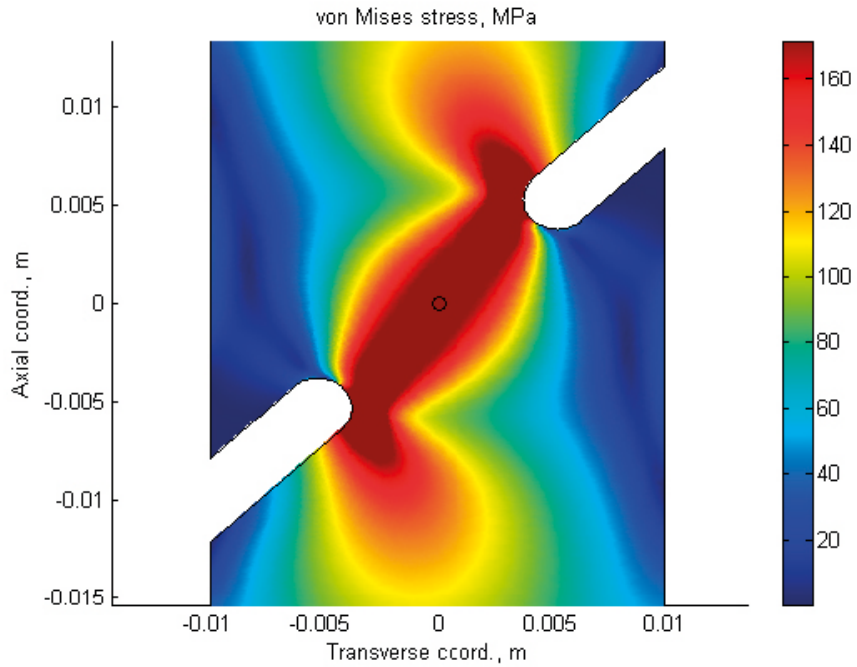

Figure 6-6. *von Mises stress distribution at collapse load around the notches for the shear specimen tested at 75°C and 80 MPa. Flow stress 173 MPa.*

6.4 Creep in compression

In Figure 4-12 results from creep testing in compression were presented. A feature that might seem surprising is that the creep results for as-received and cold worked material are about the same. When Cu-OFP is creep tested in tension there is a very large increase in creep strength after 24% cold work in tension (Wu et al. 2014). The observed increase was about 30%. However, when the cold work was carried out in compression little increase in creep strength was found. Thus, it was noted that if the cold work and creep testing were performed in the same direction the increase in strength was large, if they were in opposite direction the strength was essentially unchanged (Wu et al. 2014). In the compression tests the cold work was in tension whereas the creep testing was in compression, i.e. in opposite directions. The absence of a strength increase after cold work is consequently not very surprising. The mechanistic reason is believed to be found in the changes in the substructure. During cold working a pronounced substructure is formed that raises the strength. However, when the loading direction is reversed, the motion of the dislocations is reversed and the substructure is dissolved (Wu et al. 2014).

A creep curve for as-received Cu-OFP tested under identical conditions to those in Figure 4-12 is shown in Figure 6-7 (Andersson et al. 2007). The only difference is that the test has been performed in tension instead of compression. Model results are also shown (Sandström 2012). The cusps in the experimental curve are due to reloading of the specimen.

Figure 4-12 and Figure 6-7 appear quite different. Neither the time range nor the strain range is close. It is therefore of interest to model the curves in Figure 4-12 in the same way as Figure 6-7. The difference between testing in tension and compression is that the diameter of the specimen decreases with strain in tension whereas it increases in compression. This means that the stress gradually is raised in tension but reduced in compression. This is automatically taken into account in the stress analysis if true stresses are used. Using the same model as in Figure 6-7 (Sandström 2012) the results in Figure 6-8 are obtained.

The experimental curves in Figure 6-8 are the same as the ones in Figure 4-12. The only difference is that the strains on loading are added (12%). For comparison with the model the strains on loading must be taken into account. The model does not completely simulate the experiments. The predicted strain on loading is a little smaller (10%) and the strain variation is larger in the model curve than in the experimental curves. However, the main difference between the curves in Figure 4-12 and Figure 6-7 can clearly be explained.

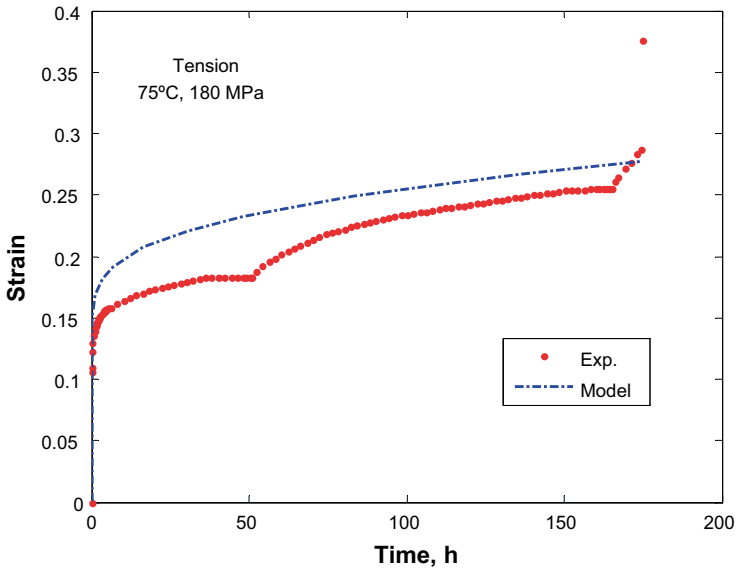

Figure 6-7. *Creep strain versus time for as-received Cu-OFP tested in tension at 75°C and at 180 MPa. Model results are also included.*

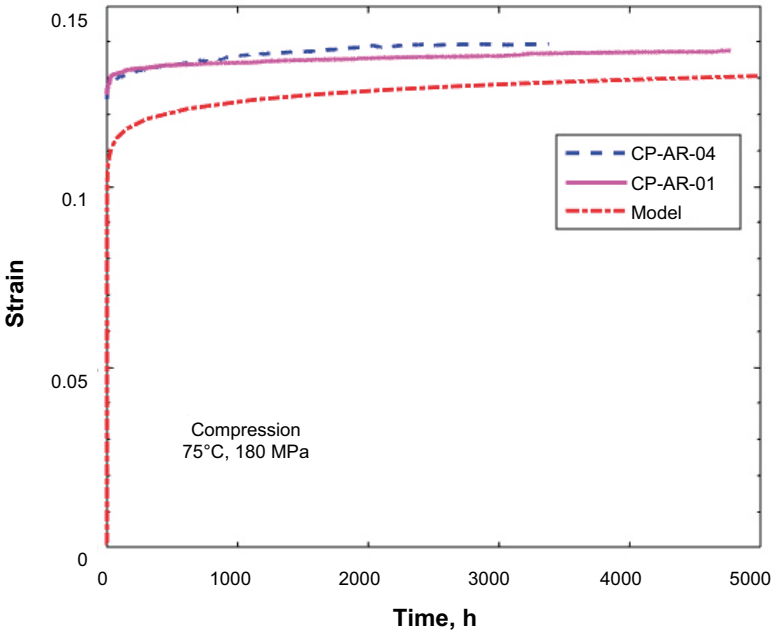

Figure 6-8. *Creep strain versus time for as-received Cu-OFP tested in compression at 75°C and at 180 MPa. Model results are also included.*

7 Conclusions

Both as-received and 24% in tension cold worked Cu-OFP materials have been investigated in terms of creep properties in the present study. Creep tests using notched specimen for the 24% cold worked Cu-OFP, CCG tests using CT specimen with or without side grooves for the as-received Cu-OFP, shear tests using shear specimen with 45° notch to the axial direction for the as-received Cu-OFP, and compression tests using columnar specimen for both the as-received and the 24% cold worked Cu-OFP have been performed. The following conclusions can be drawn:

1) The creep lifetime for the notched 24% cold worked Cu-OFP is considerable longer than for notched as-received Cu-OFP. The increase in strength is at least as large as that observed for cold worked uniaxial specimens, namely 30%. The strength estimated with the reference stress method does not overestimate the rupture strength. The 24% cold worked Cu-OFP is clearly insensitive to notches at 75°C.
2) For the tests using CT specimens without side grooves at 75, 100, 125 and 175°C, no significant crack initiation was seen at interruption. For the test using CT specimen with side grooves at 125°C, crack formation and propagation were observed. A previously developed model could at least qualitatively describe the amount of crack propagation. No propagation was predicted for the specimens without side grooves, but significant propagation for the specimen with side grooves. Together with previous results this demonstrates that highly constrained notches with a pronounced multiaxial stress state give rise to crack initiation in Cu-OFP at 125°C and higher temperatures.
3) CT specimens used for CCG tests were strongly bent at interruption due to the low strength and good ductility of Cu-OFP material. Grains adjacent to notches have been noticeably deformed. This is more pronounced in the middle than that at sub-surface of the CT specimen.
4) Creep damage in form of intergranular cracks and cavities was found close to and away from the notch in the CT specimens. The presence of creep cavitation indicates that crack propagation takes place by creep damage formation, which is precisely what is assumed in the model for crack propagation.
5) Extent and degree of creep cavities and cracks decrease with decreasing temperature as well as with increasing distance from the notch tip. At 100°C and below, limited creep cavities are observed no more than 2 mm from notch tip.
6) The apparent difference between uniaxial tests in tension and compression can be explained by the difference in the time dependence of the stress.
7) The shear specimens represented a simplified geometry and conditions in the slits of the canister. It is demonstrated that the rupture strength of the specimens can be predicted with the reference stress method.

8 Acknowledgements

This work has been performed at Swerea KIMAB. SKB is thanked for providing the test material. Members from the research committee, Christina Lilja, Håkan Rydén, Mikael Jonsson, Matts Björck, all from SKB, and Henrik Östling, Swerea KIMAB, are thanked for discussions and comments. Facredin Seitisleam and Mats Larsson, Swerea KIMAB, are thanked for carrying out creep tests.

References

SKB's (Svensk Kärnbränslehantering AB) publications can be found at www.skb.se/publications.

Andersson H, 2005. Creep crack propagation in pure copper at 75°C. IM-2005-130, Corrosion and Metals Research Institute, Sweden.

Andersson H C M, Seitisleam F, Sandström R, 2007. Creep testing and creep loading experiments on friction stir welds in copper at 75°C. SKB TR-07-08, Svensk Kärnbränslehantering AB.

ASTM E-1457-98. Standard test method for measurement of creep crack growth rates in metals. 2nd draft version. West Conshohocken, PA: ASTM International.

Auerkari P, Holmström S, Salonen S, Nenonen P, 2005. Creep performance of OFP copper for the overpack of repository canisters. In Van Iseghem P (ed). Scientific basis for nuclear waste management XXIX: proceedings of a meeting held in Ghent, Belgium, 12–16 September 2005. Warrendale, PA: Materials Research Society. (Materials Research Society Symposium Proceedings 932), 885–892.

Auerkari P, Rantala J, Salonen J, 2009. Effect of defects on low temperature creep of OFP copper. In Shibli I A, Holdsworth S R (eds). Creep and fracture in high temperature components: proceedings of the 2nd ECCC Conference, Zurich, Switzerland, 21–23 April 2009, 287–297.

Dyson B F, Loveday M S, 1981. Creep fracture in Nimonic 80A under triaxial tensile stressing. In Ponter A R S, Hayhurst D R (eds). Creep in structures: proceeding of the 3rd Symposium, Leicester, UK, 8–12 September 1980. Oxford: Pergamon, 406–421.

Hayhurst D R, Henderson J T, 1973. Creep stress redistribution in notched bars. International Journal of Mechanical Sciences 19, 133–146.

Hayhurst D R, Webster G A, 1986. An overview on studies of stress state effects during creep of circumferentially notched bars. In Gooch D J, How I M (eds). Techniques for multiaxial creep testing. London: Elsevier Applied Science, 137–175.

ISO EN 204:2005. Metallic materials – Uniaxial creep testing in tension – Method of test. Geneva: International Organization for Standardization.

Jin L-Z, Sandström R, 2013. Influences of load variations on the plastic deformation in friction stir welds and contour slits in copper shells. SKB TR-13-25, Svensk Kärnbränslehantering AB.

Miller A G, 1988. Review of limit loads of structures containing defects. Review of limit-loads of structures containing defects 32, 197–327.

Rosborg B, Werme L, 2008. The Swedish nuclear waste program and the long-term corrosion behaviour of copper. Journal of Nuclear Materials 379, 142–153.

Sandström R, 2012. Basic model for primary and secondary creep in copper. Acta Materialia 60, 314–322.

Sandström R, Andersson H, 2008. Creep in phosphorus alloyed copper during power-law breakdown. Journal of Nuclear Materials 372, 76–88.

Seitisleam F, Henderson P, 1997. Creep of copper for nuclear waste containment – results of testing performed in 1996. IM-3506, Corrosion and Metals Research Institute, Sweden.

SKB, 2010. Design, production and initial state of the canister. SKB TR-10-14, Svensk Kärnbränslehantering AB.

Webster G A, Ainsworth R A, 1994. High temperature component life assessment. London: Chapman & Hall.

Webster G A, Aplin P F, Cane B J, Dyson B F, Loveday M S, 1992. A code of practice for notched bar creep rupture testing: procedures and interpretation of data for design. In Loveday M S, Gibbons T B (eds). Harmonisation of testing practice for high temperature materials. London: Elsevier Applied Science, 295–330.

Wu R, Seitisleam F, 2010. Creep crack growth in phosphorus alloyed oxygen free copper. KIMAB-2010-102, Swerea KIMAB.

Wu R, Jin L-Z, Sandström R, 2009a. Influence of multiaxial stresses on creep properties of phosphorus alloyed oxygen free copper, Proceedings of PVP 2009, 2009 ASME Pressure Vessels and Piping Division Conference, Prague, Czech Republic, 26–30 July 2009.

Wu R, Seitisleam F, Sandström R, 2009b. Creep properties of phosphorus alloyed oxygen free copper under multiaxial stress state. SKB R-09-41, Svensk Kärnbränslehantering AB.

Wu R, Sandström R, Jin L-Z, 2013. Creep crack growth in phosphorus alloyed oxygen free copper. Materials Science and Engineering A 583, 151–160.

Wu R, Pettersson N, Martinsson Å, Sandström R, 2014. Cell structure in cold worked and creep deformed phosphorus alloyed copper. Materials Characterization 90, 21–30.

Arkitektkopia AB, Bromma, 2018

SKB is responsible for managing spent nuclear fuel and radioactive waste produced by the Swedish nuclear power plants such that man and the environment are protected in the near and distant future.

skb.se